

Optimized delivery of intensity-modulated radiotherapy

Dissertation

zur Erlangung des Grades eines Doktors
der Naturwissenschaften
der Fakultät für Physik
der Eberhard-Karls-Universität zu Tübingen

vorgelegt von

Werner Bär
aus Erlangen

2002

Tag der mündlichen Prüfung:	24. Oktober 2002
Dekan:	Prof. Dr. H. Müther
1. Berichterstatter:	Prof. Dr. F. Nüsslin
2. Berichterstatter:	Prof. Dr. W. Schlegel

Zusammenfassung

In der Strahlentherapie werden hochenergetische Photonenstrahlen aus meist unterschiedlichen Einstrahlrichtungen zur Tumorbekämpfung verwendet. Die Strahlenbündel werden präzise auf den Tumor fokussiert um umliegendes Normalgewebe zu schonen. Hierzu werden vor allem Multilamellen-Kollimatoren (MLCs) benutzt, bei denen die gewünschte Form des Strahlenfeldes durch schmale, bewegliche Wolfram-Lamellen computer-gesteuert angenähert werden kann. Heutzutage kommen MLCs mehr und mehr für Behandlungen mit fluenzmodulierter Strahlentherapie (IMRT) zum Einsatz. Im Gegensatz zur konventionellen Bestrahlung moduliert IMRT die Fluenz des Photonenstrahls innerhalb des Bestrahlungsfeldes. Dieser neue Freiheitsgrad ermöglicht es, tumor-konformere Dosisverteilungen zu erlangen und damit die zu erwartenden Komplikationen für das Normalgewebe zu senken oder die Tumordosis zu steigern ohne das Normalgewebe stärker zu gefährden. Diese noch relativ junge Technik hat sich in den letzten 10 Jahren zum bedeutendsten neuen Konzept der Strahlentherapie entwickelt, und bis zum Jahre 2000 wurden weltweit bereits etwa 5000 Patienten mit IMRT behandelt [58]. Während sich ihr Einsatz vor einigen Jahren noch auf einige wenige Forschungszentren beschränkt hat, wird IMRT mittlerweile mehr und mehr auch in der klinischen Routine eingesetzt. Obwohl sich die Bestrahlungsplanung von IMRT auch mit konventioneller Vorwärtsplanung umsetzen läßt, wird IMRT zumeist mit inverser Planung kombiniert. Bei dieser wird eine erwünschte, ideale Dosisverteilung im Vorfeld verschrieben, und ein Computer-Algorithmus erzeugt anschließend realisierbare, fluenzmodulierte Photonenfelder, die diese Verteilung so gut wie möglich approximieren.

IMRT kann auf unterschiedliche Art und Weise mit einem MLC umgesetzt werden. Eine Methode ist die statische Multilamellen-Kollimation (sMLC), bei der aus jeder Einstrahlrichtung mehrere Einzelfelder mit unterschiedlicher Feldform durch Überlagerung die Fluenzmodulation bewirken. Da diese Technik relativ einfach und der konventionellen Therapie ähnlich ist, hat sich sMLC zu einem der wichtigsten Verfahren zur Applikation von IMRT entwickelt. Um Behandlungen mit sMLC durchführen zu können ist es notwendig, jedes fluenzmodulierte Feld in eine Reihe von Einzelfelder zu zerlegen, die mit dem MLC appliziert werden können. Dieser Vorgang wird üblicherweise in zwei Schritten vollzogen. Zunächst wandelt die Gruppierung das ideale, meist quasi-kontinuierliche Feldprofil in ein stückweise konstantes Profil mit wenigen Stufen um. Anschließend wird dieses durch die Segmentierung in Einzelfelder bzw. Segmente transformiert, die das gruppierte Profil durch Überlagerung reproduzieren.

Gruppierung und Segmentierung modifizieren die optimierten Fluenzverteilungen und verschlechtern die Dosisverteilung. Da sie üblicherweise als letzter Schritt der Bestrahlungs-

planung durchgeführt werden, sind die eingeführten Modifikationen der Dosisverteilung unkontrolliert und können die erwarteten Behandlungsergebnisse drastisch verschlechtern und zu einem klinisch nicht akzeptablen Behandlungsplan führen. Diese Problematik ist um so gravierender, falls Gruppierung und Segmentierung nicht speziell an die oftmals komplexen technischen Beschränkungen des verwendeten MLC-Typs angepaßt sind.

In der vorliegenden Arbeit wurde ein neuer Algorithmus für Gruppierung und Segmentierung entwickelt. Beide sind speziell auf die technischen Bedingungen eines bestimmten MLC-Typs zugeschnitten, um sowohl die notwendigen Modifikationen als auch die Anzahl der resultierenden Segmente zu minimieren. Der Algorithmus wurde in die inverse Planung, d.h. in den gesamten Prozess der Optimierung der Dosisverteilung, integriert. Die Modifikationen der Dosisverteilung durch Anwendung von Gruppierung und Segmentierung auf die idealen, fluenzmodulierten Felder werden auf diese Weise von der inversen Bestrahlungsplanung kontrolliert. Mit dieser grundlegenden Verbesserung ist es möglich, Bestrahlungspläne zu erzeugen, die der ursprünglichen Dosisverschreibung entsprechen. Unser Konzept hat sich in mehreren Planungsstudien bewährt und wird seit Oktober 2001 in der Universitätsklinik Tübingen zur Behandlung von Prostata- und seit Mai 2002 auch von Kopf-Hals-Tumoren verwendet.

In **Kapitel 2** werden zunächst einige grundlegende Begriffe und Definitionen eingeführt. Anschließend wird auf die Entwicklung und Verwendung von MLCs eingegangen und einige unterschiedliche MLC-Typen werden vorgestellt. Insbesondere werden die wesentlichen Eigenschaften des für diese Arbeit wichtigen MLCs der Firma Elekta detailliert dargestellt.

In **Kapitel 3** werden unterschiedliche Methoden vorgestellt, IMRT mit einem MLC umzusetzen. Neben den wichtigsten Eigenschaften der jeweiligen Technik werden deren spezifische Vor- und Nachteile sowie deren klinische Verbreitung erläutert.

In **Kapitel 4** wird näher auf das Verfahren der Gruppierung eingegangen. Zunächst wird eine der Standard-Techniken, die Bortfeld-Boyer-Methode, vorgestellt. Bei diesem Verfahren werden die quasi-kontinuierlichen Profile auf stückweise konstante Profile mit fester Stufenhöhe projiziert. Die Beschränkung auf äquidistante Fluenzstufen limitiert auf diese Weise die Möglichkeiten, die idealen Profile genau anzunähern. In der vorliegenden Arbeit wurde ein neuer Algorithmus entwickelt, der variable Stufenhöhen verwendet, um diesen Nachteil zu vermeiden. Weiterhin sorgt unsere Gruppierungs-Strategie für stückweise konstante Profile, die den Beschränkungen des Elekta MLCs gehorchen und sich somit ohne weitere Modifikationen in Segmente zerlegen lassen. Eine Vergleichsstudie der beiden Techniken für zahlreiche mathematische und klinische Beispielprofile demonstriert die Möglichkeiten unserer Methode, ideale Profile genauer durch realisierbare approximieren zu können.

In **Kapitel 5** wird die neue Methode der Segmentierung detailliert vorgestellt. Neben den Grundzügen des Algorithmus wird genauer auf die Berücksichtigung der technischen

Beschränkungen des Elekta MLCs, auf die Optimierung der Segmentformen und die Berechnung der Lamellenpositionen eingegangen. Die resultierenden Segmente werden sortiert, um die notwendigen Lamellenbewegungen zwischen den einzelnen Segmenten zu minimieren und Verifikations-Aufnahmen des Gesamtfeldes zu Beginn der Bestrahlung zu ermöglichen. Spezielle Routinen können eingesetzt werden, um die unwichtigsten Segmente in Bezug auf Gewicht oder Größe zu eliminieren und mehrere Segmente mit anderen Segmenten zu verbinden. Ziel dieser Methoden ist die Steigerung der Effizienz der Behandlung und die Senkung der Komplexität der Qualitätssicherung. Anschließend wird auf einige generelle Eigenschaften der Segmentierung eingegangen, wie etwa die Berücksichtigung des Tongue&Groove-Effekts. Die Effizienz unseres Algorithmus wird anhand der Segmentierung von zahlreichen gruppierten Profilen demonstriert.

In **Kapitel 6** wird zunächst die Bedeutung der Integration von Gruppierung und Segmentierung in die Optimierung der Dosisverteilung erläutert. Nach der Vorstellung der Grundzüge der inversen Bestrahlungsplanung mit dem in unserer Abteilung entwickelten Programm HYPERION wird unser Konzept zur Integration erläutert. Um einen ersten, geeigneten Satz von Segmenten zu erlangen, werden zuerst ideale Fluenzprofile optimiert und eine erste Gruppierung und Segmentierung durchgeführt. Anschließend werden die Segmentformen und -gewichte in der Nachoptimierung der Segmente berücksichtigt. Abschließend ergeben sich somit applizierbare Segmente, die eine Dosisverteilung erzeugen, die den Anforderungen der verordneten Dosisverschreibung genügt.

In **Kapitel 7** werden Ergebnisse der Bestrahlungsplanung mit integrierter Gruppierung und Segmentierung präsentiert und die klinische Anwendung unserer Methode erläutert. Zunächst wird eine Studie, die den Zusammenhang zwischen der Qualität der Dosisverteilung und der Anzahl der Segmente untersucht, vorgestellt. Die Ergebnisse demonstrieren die Effizienz unseres Konzepts, mit einer hinreichend geringen Anzahl von weniger als 50 Segmenten auch in komplexen Fällen sehr gute Dosisverteilungen zu erzeugen. Anschließend veranschaulicht eine Vergleichsstudie unserer Strategie mit einem Vorwärtsplanungskonzept mit Nachoptimierung der Segmentgewichte für 10 Patienten mit Kopf-Hals-Tumoren die signifikanten Vorteile der vollständig inversen Planung in Bezug auf die Qualität der Dosisverteilung. In einer dritten Studie wird unser Konzept der integrierten inversen Planung mit einer konventionellen Methode, bei der Gruppierung und Segmentierung nach abgeschlossener Optimierung zum Einsatz kommen, für einen komplexen Kopf-Hals-Fall verglichen. Während die konventionelle Strategie die klinischen Erfordernisse in Bezug auf Dosisverteilung und Segmentzahl klar verfehlt, ergibt sich mit unserer Methode ein geeigneter Behandlungsplan. Diese Ergebnisse belegen den Wert unseres Konzepts für klinisch adäquate und effiziente inverse Planung. Abschließend werden die ersten Ergebnisse der klinischen Anwendung unseres IMRT-Konzepts zur Behandlung von Patienten mit Prostata- und seit kurzem auch Kopf-Hals-Tumoren kurz vorgestellt.

Contents

1	Introduction	1
2	Multileaf Collimator	4
2.1	Terminology	4
2.2	Development and Clinical Usage	6
2.3	The Elekta Multileaf Collimator	8
2.3.1	Design	8
2.3.2	Performance Characteristics	10
2.4	Other Types of Multileaf Collimators	11
3	Intensity-Modulated Radiotherapy with an MLC	13
3.1	Static Multileaf Collimation	14
3.2	Dynamic Multileaf Collimation	17
3.3	Intensity-Modulated Arc Therapy	19
3.4	Tomotherapy	20
4	Clustering	22
4.1	The Bortfeld-Boyer Method of Clustering	22
4.2	Clustering Algorithm	23
4.3	Modifications of the Clustered Profiles	25
4.4	Performance of the Clustering	26
5	Segmentation	30
5.1	Segmentation Algorithm	31
5.1.1	Concept	31
5.1.2	Preparation	31
5.1.3	Segmentation	33
5.1.4	Leaf Positions	36
5.1.5	Superimposition of Segments	37
5.1.6	Merging of Segments	38

5.1.7	Sorting of Segments	39
5.2	Reduction of the Number of Segments	40
5.2.1	Minimum Segment Weight Constraint	40
5.2.2	Minimum Segment Size Constraint	41
5.2.3	Extended Merging	41
5.2.4	Extended Superimposition	41
5.3	Features of the Segmentation Algorithm	43
5.3.1	Sliding-Window vs. Close-In	43
5.3.2	Tongue&Groove-Effect	44
5.3.3	Approximation of the Clustered Profiles	44
5.4	Performance of the Segmentation	45
6	Integration into the Inverse Planning Algorithm	46
6.1	Inverse Planning	47
6.2	Re-Optimization of Segments	48
6.3	Integration of the Sequencing	50
7	Performance of the Integrated Sequencer	51
7.1	Efficiency of Integrated Segment Optimization	51
7.2	Forward vs. Inverse Planning	53
7.3	Conventional vs. Integrated Sequencing	56
7.4	Tongue&Groove-Effect	61
7.5	Clinical Implementation	61
8	Conclusion	62
A	Paper: Clustering and Segmentation Algorithm	74
B	Paper: Performance of the Integrated Sequencer	86

Chapter 1

Introduction

Radiotherapy can be delivered with e.g. photons, electrons or protons. Irradiation with these particles aims at shaping the dose distribution conformally to the tumor while sparing normal tissue. Conventional radiotherapy usually uses photons beams from multiple directions but with constant intensity from each incidence. *Intensity-modulated radiotherapy* (IMRT)¹ employs an additional degree of freedom by modulating the photon fluence within the radiation field [14]. Conventional radiotherapy is usually performed with *forward planning*, where the beam directions and intensities are defined from which the resulting dose distribution is calculated. The distinctly more complex concept of IMRT led to the development of *inverse treatment planning*, where the desired dose distribution is specified in advance and field intensities which approximate this dose distribution are calculated subsequently. Furthermore, the introduction of IMRT was accompanied by the development of new treatment devices like the *multileaf collimator* (MLC) [13]. In the mid 1990s, some centers started to treat patients with IMRT [36, 52]. Since then, IMRT has become without doubt the most important new technique in the field of radiotherapy and by the year 2000 about 5000 patients had been treated with IMRT worldwide [58]. There is general agreement that IMRT has not only the potential to improve dose distributions but also treatment outcomes significantly. First clinical results are promising [50, 90].

At present, clinical IMRT is no longer restricted to research centers and has found widespread usage in numerous hospitals. As a consequence, the research topics have shifted: While in the early days of IMRT the main focus was on solutions to plan and deliver it in principle, nowadays it is on practical and efficient strategies for the use in clinical routine. One of the established methods to deliver IMRT with an MLC is *static multileaf collimation* (sMLC), where a series of fields, henceforth denoted as *segments*, from each beam direction are superimposed to achieve an intensity-modulated field [10].

¹According to radiation physics nomenclature it is the fluence rather than the intensity of a beam which is modulated. However, the more popular term intensity is used synonymously in this work to avoid confusion with the literature.

The major advantage of sMLC is its close relation to conventional radiotherapy. Therefore, its clinical introduction can build on existing procedures and know-how. Treatment planning for sMLC is usually performed in two steps: At first, inverse planning generates an optimized treatment plan. Afterwards, this plan is modified due to the technical limitations and characteristics of the MLC. Typically, the transformation of the optimized into a deliverable treatment plan, in what follows referred to as *sequencing*, neither considers dosimetric parameters nor is it specifically designed for the MLC that is used for treatment. In this way, the introduced deviations between optimized and deliverable dose distribution are not controlled at all and the sequencing will generally deteriorate the dose distribution significantly. As a consequence, aims of the treatment that were initially met will often finally be missed and treatment plans may not be clinically acceptable any more. Furthermore, this concept may on the one hand lead to impractical segments in terms of size, weight, shape or position, on the other hand to an immense number of segments. In this way, lengthy delivery times, complicated quality assurance and increased influence of leakage and head scatter may result.

A plausible but challenging way to eliminate these drawbacks is to use a concept of sequencing which accounts for the technical limitations of the MLC during the optimization of the dose distribution. The aim of this strategy of optimization with integrated sequencing is to no longer produce undeliverable, theoretical fluence profiles, but implementable MLC parameters. In this thesis, a sequencer with such characteristics was developed:

- A new method of approximating the optimized, freely modulated *fluence weight* distributions by deliverable ones is presented. In particular, the strategy aims at minimizing the introduced modifications by using variable fluence weight increments instead of equidistant levels for the approximation. A comparison with the conventional strategy for several test cases demonstrates the superiority of the method.
- A new approach of determining the series of segments for the application of the deliverable treatment plan is introduced. It was specifically designed for the MLC model used at the University Hospital of Tübingen (UKT), but the strategies developed for this specific MLC can also be applied to other designs in a slightly modified way. The method takes considerations about the shape and weight of the segments into account to force the algorithm to end up with reasonable segments from a technical and clinical point of view. Further strategies aim at eliminating the dosimetrically least important segments to reduce the treatment time. A study proves the efficiency of our algorithm.
- The sequencer was integrated into the inverse planning algorithm developed at the UKT to be able to consider the series of segments during the optimization of the dose distribution. Modifications due to the sequencing are compensated for and the final

dose distribution satisfies the dose prescription. The performance characteristics of inverse planning with the integrated sequencer demonstrate the potential to optimize treatment plans with respect to the quality of the dose distribution. Furthermore, it can be shown that our concept is superior to forward planning for complex cases and to conventional inverse planning in general. In the sequel of these findings, our inverse planning method has been clinically implemented at the UKT to treat patients with prostate and head&neck tumors.

Chapter 2

Multileaf Collimator

Radiotherapy is usually performed with high-energy X-rays generated by a *linear accelerator*, where electrons with energies of typically 4-25 MeV hit a tungsten *target* to create Bremsstrahlung X-rays¹. The photon beam is filtered and focussed by attenuating material to achieve a constant intensity and a well-defined geometry. The patient is positioned on a *treatment table* which can be moved and rotated. The linear accelerator consists of a revolving radiation head denoted as *gantry*, which can be rotated about a horizontal axis to adjust the desired *beam direction*. A treatment usually consists of irradiation from different gantry positions. A sketch of the principle of radiotherapy with a linear accelerator is given in figure 2.1. One major issue of the treatment is to direct the photons towards the tumor and to shield the surrounding normal tissue as well as possible. The penetration depth within the patient can be tuned by the choice of the photon energy. In this chapter, methods to laterally focus respectively block the photon beam are discussed. First of all, some terminology is introduced, which is used throughout this thesis.

2.1 Terminology

An electron beam with a mean energy of e.g. 6 MeV creates a continuous spectrum of Bremsstrahlung X-rays with a maximum energy of 6 MeV. These photons are denoted as 6 MV photons. A number of *monitor units* specifies the amount of irradiation and is attributed to every photon beam. The *dose rate* determines the amount of monitor units irradiated per time interval. The *central ray* of the beam hits the *isocenter*, a point within the patient which matches the center of rotation of gantry and treatment table. The view from the photon source along the central ray towards the patient is referred to as *beam's eye view* (BEV). The plane through the isocenter perpendicular to the central ray is called *isocentric plane*. In what follows, geometrical dimensions perpendicular to the central

¹The target is therefore also referred to as the *source* of the photons.

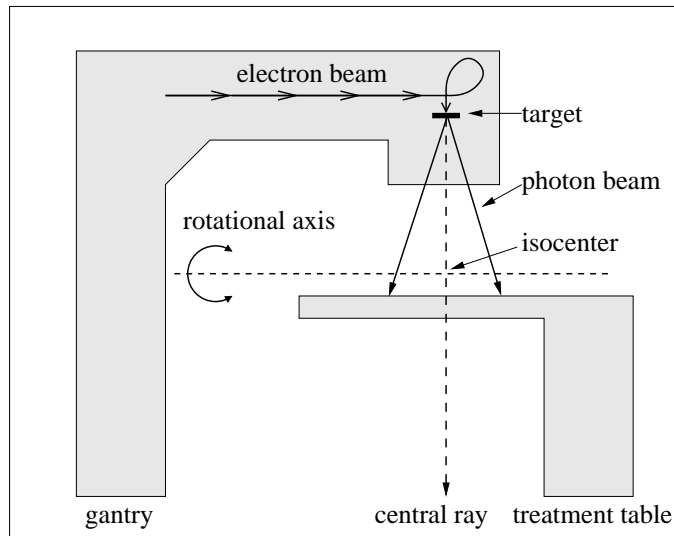


Figure 2.1: Sketch of the principle of radiotherapy with a specific linear accelerator. The electrons are bent by a 270° magnet and directed towards the tungsten target to create the X-rays.

ray are always discussed in the isocentric plane if not explicitly mentioned differently. In contrast to the borders of the *light field*, the edges of the *radiation field* have a rather broad and continuous transition between fully irradiated and fully blocked regions due to transmission and scatter of the photons. The partially irradiated area is denoted as *penumbra* and quantified in percentage of the dose of the fully irradiated regions.

The distribution of the photon beam as function of energy, position and direction in planes tangential to a sphere centered at the photon source is referred to as *fluence distribution* $\Phi(E, \phi, \theta, x, y)$. As the fluence distribution cannot be measured or manipulated directly, the clinically relevant quantity is the *fluence weight distribution*, which assigns an irradiation time to every elementary fluence distribution that can be produced technically. In this sense, a fluence weight distribution is obtained from a fluence distribution by a weighted superimposition of elementary fluence elements, which can be segments or *beamlets*. A beamlet is the smallest difference of two fluence distributions that can be delivered by shifting one MLC leaf. The unit of the fluence weight distribution is monitor units. In what follows, fluence weight distributions are also denoted as *fluence weight profiles*. The distribution of the energy deposition of the photon beam within the patient volume is denoted as *dose distribution*. The relation between fluence weight and dose distribution is in general quite complex, because it is influenced by the geometry and density distribution of the patient. The patient is divided into tumor and normal tissue volumes. The volume to be irradiated is called the *planning target volume* (PTV). It consists of the primary tumor, volumes with suspected, subclinical disease and safety margins to account for geometrical

variations to ensure an appropriate application of the prescribed dose. Very dose-sensitive parts of the normal tissue which may restrict the acceptable tumor dose are denoted as *organs at risk* (OARs).

Finally, three different time intervals are distinguished. The *beam-on time* specifies exclusively the time periods, when the irradiation is explicitly on. The *irradiation time* denotes the time interval between start of the irradiation of the first field until the end of the irradiation of the last field. In this way, it also includes the time to e.g. rotate the gantry. The total time necessary to deliver a radiotherapy treatment is referred to as *treatment time* and consists of the irradiation time as well as e.g. procedures for patient setup.

2.2 Development and Clinical Usage

Conventional radiotherapy with a linear accelerator, as it has been used in clinical routine during the last decades, is usually performed with four *diaphragms* to set the boundaries of the radiation field. The diaphragms can be moved independently to encompass the projection of the PTV and to shield the surrounding tissue as seen in BEV. As only linear movement of the diaphragms is permitted, the geometry of the radiation field is restricted to rectangular shapes (see figure 2.2 a). The maximum field size is usually limited to $40 \times 40 \text{ cm}^2$, which is sufficient for most treatments.

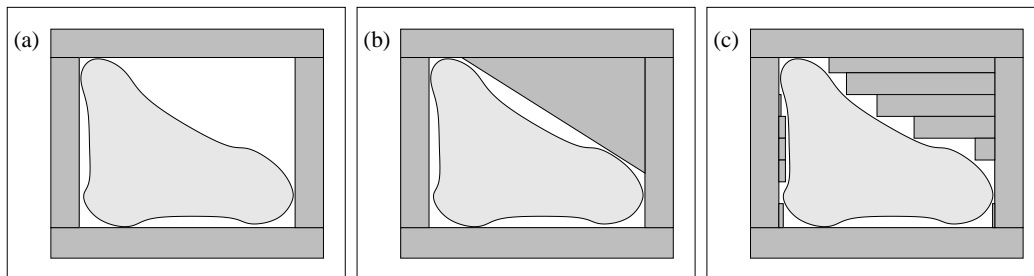


Figure 2.2: Examples of different shielding techniques for the treatment of a tumor as seen from BEV (the attenuating elements are illustrated in dark gray, the tumor in light gray). Conventional blocking with 4 diaphragms defines a rectangular field that encompasses the tumor and a large amount of normal tissue (a). Conformal radiotherapy uses either an additional block (b), or a computer-controlled MLC (c) to shield normal tissue. Notice that the MLC employs stepped leaf positions to approximate a diagonal contour, while the block is individually manufactured to align with the tumor shape.

Rectangular fields are never a good approximation of the tumor shape and a large amount of normal tissue may be irradiated in addition to the tumor (see figure 2.2 a). As a consequence, improved shielding of normal tissue has become a major issue since the 1980s. In particular, *conformal radiotherapy* aims at enhanced blocking of OARs, as this

may either reduce the normal tissue complications or allow a higher tumor dose. New methods to block radiation have been introduced for conformal radiotherapy. Initially, moulded blocks of metal were used as additional radiation shields and attached to the treatment machine below the diaphragms. In this way, it is possible to modify the field boundaries, so that they conform more closely to the tumor. In figure 2.2 b, an example of a conformal field defined by the diaphragms and an additional block is presented. These blocks have to be individually manufactured for each patient. Beside the time- and labour-consuming manufacturing of blocks and the need for storage rooms, the use of blocks has additional disadvantages. First of all, the procedure of lifting and attaching the heavy blocks increases the risk of injury for the clinical staff and limits the weight of the blocks. As a consequence, blocks have a smaller thickness than the diaphragms and shielding is less effective. Furthermore, treatments with blocks are time-consuming, because the clinical staff has to enter the treatment room and replace the blocks [11].

These disadvantages of blocks motivated the development of the multileaf collimator. Although the idea is decades old, the first prototypes of modern computer-controlled MLCs were built about 15 years ago and MLCs are commercially available since the early 1990s [8, 13, 74]. The main part of the MLC consists of two opposing banks of small attenuating elements which are denoted as *leaves*. Each leaf is fully computer-controlled and can be moved individually to conform the MLC-field to the specific shape of the tumor (see figure 2.2 c). The use of an MLC for conformal radiotherapy eliminates some of the shortcomings of blocks. Manufacturing, storage and lifting of heavy objects is avoided. There is no need for the clinical staff to enter the treatment room to rearrange the field shapes. Furthermore, MLC-leaves can be fabricated with the same thickness as conventional diaphragms [11].

An MLC-field is an approximation of the contour of the PTV. Several concepts for field shaping with an MLC are used. One can specify the leaf positions, so that no leaf blocks any part of the PTV, or so that the surrounding normal tissue is completely shielded from irradiation, or so that there is a trade-off between irradiation of the tumor and blocking of normal tissue [91]. Leaf positioning can be optimized with respect to geometrical alone or geometrical and dosimetric aspects [38, 54, 71, 89]. Generally, the approximation of the desired field contour by the MLC-leaves is more difficult, if the desired field edge is neither roughly parallel nor perpendicular to the leaf ends. The worst case scenario is an angle of 45° between the desired field edge and the leaf ends. In this case, the straight field edge has to be approximated by stepped leaf positions as demonstrated in figure 2.2 c. The influence of stepped leaf positions has been investigated with regard to the penumbra [11, 38, 44, 59]. Due to transmission and scatter, the modulation of the isodose lines is less pronounced than the modulation of the light field. However, the stepped leaf positions increase the penumbra by a few millimeters. In most cases, this effect is not clinically significant for

the cumulative dose distribution, because it is smeared out due to the superimposition of several fields.

At present, field shaping with an MLC is the method of choice of delivering conformal radiotherapy and the number of MLCs in clinical use has been growing fast during the last ten years [78].

2.3 The Elekta Multileaf Collimator

The work of this thesis concerns radiotherapy with an Elekta MLC in particular. The following section provides some important information about this MLC. Further details can be found in the MLC-manual [34] and in a publication by Jordan and Williams [46].

2.3.1 Design

The Elekta MLC is commercially available since the early 1990s. It replaces the conventional radiation head and fits inside the head cover, weighing 245 kg with a depth and width of 62 cm and a height of 42 cm. The MLC consists of 40 pairs of leaves, which are evenly divided among two opposing leaf banks, a pair of x-diaphragms and a pair of y-diaphragms. All components are made of tungsten alloy. The leaves have a thickness of 7.5 cm, the x-diaphragms of 7.0 cm and the y-diaphragms of 3.0 cm.

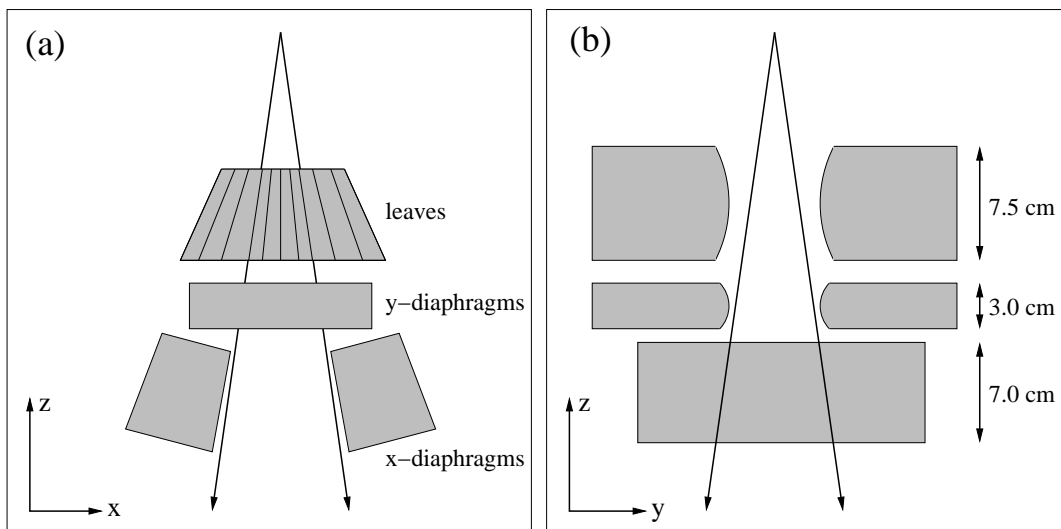


Figure 2.3: Photons are emitted from the source above and pass leaves, y-diaphragms and x-diaphragms before they hit the patient below. X-diaphragms are focused towards the source, while leaves and y-diaphragms have rounded ends. (a) shows a sketch of the xz -plane which is rotated by 90° against (b), which illustrates a sketch of the yz -plane.

Figure 2.3 shows a sketch of the configuration of the MLC from two different direc-

tions. Photons are emitted from the source above, pass leaves, y-diaphragms and finally x-diaphragms, before they hit the patient below. In x-direction, movement of the x-diaphragms and the design of the leaf sides are focused towards the source (see figure 2.3 a). As a consequence, the penumbra in x-direction is independent of the exact position of leaves and diaphragms. In y-direction, leaves and y-diaphragms move along a straight line and have curved ends as illustrated in figure 2.3 b. The rounded design acts as a virtual focus, so that the penumbra is almost independent of the position of the field edge in y-direction [46]. The sides of the leaves are stepped to reduce leakage between adjacent leaves (see figure 2.4). Therefore, the projection of a single leaf has a width of 11 mm in the isocentric plane, while the projection of a missing leaf has a width of only 10 mm.

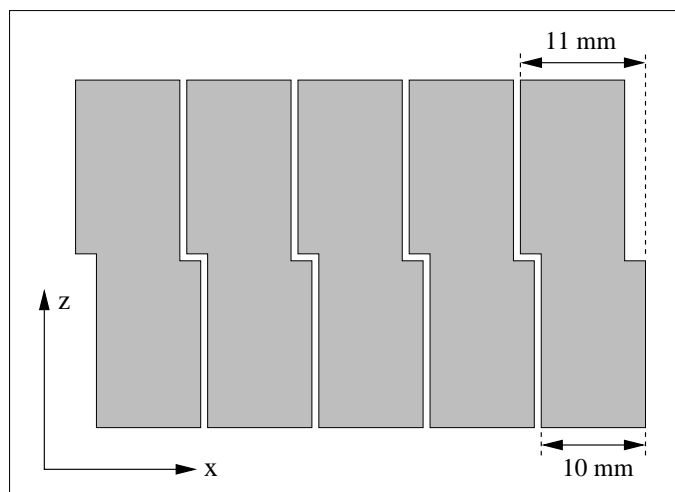


Figure 2.4: Design of the leaf sides to prevent inter-leaf leakage. In the isocentric plane, the projection of a single leaf with a width of 11 mm is slightly larger than the projection of a missing leaf with a width of 10 mm. Notice that this sketch is a simplified illustration, because the leaves are in reality focused towards the source in x-direction as shown in figure 2.3 a.

All leaves can be moved independently with a maximum velocity of 15 mm/s. They can be driven back for 20 cm in their half field, while travel in the other half is restricted to 12.5 cm. The latter restriction is referred to as *maximum overtravel constraint*. Opposing and opposing adjacent leaves can not completely close or pass each other, but must maintain a minimum distance of typically 0.5-1.0 cm, depending on the specific machine settings. The limitation for opposing leaves is denoted as *minimum gap constraint*, that for opposing adjacent leaves as *interdigitation constraint*. These restrictions are intended to guarantee trouble-free functionality of the MLC by avoiding e.g. leaf collisions due to the rounded ends. Sketches to illustrate these three constraints are given in figure 2.5.

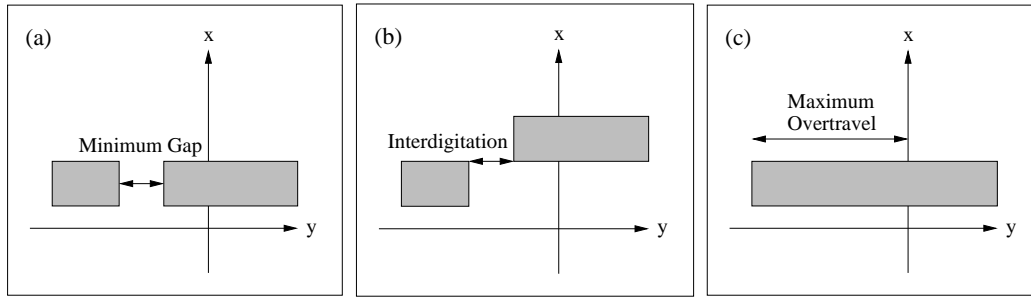


Figure 2.5: Sketches of the three important constraints of the Elekta MLC. (a) demonstrates the minimum gap constraint for two opposing leaves (illustrated in dark gray), (b) the interdigitation constraint for two opposing adjacent leaves and (c) the maximum overtravel constraint for a single right leaf.

The y-diaphragms have to satisfy the same maximum overtravel and minimum gap constraint and can be moved with a maximum speed of 20 mm/s. They are designed to reduce inter-leaf leakage and are usually positioned at the outermost field edges. However, any combination of leaf- and diaphragm-positions that satisfies the aforementioned constraints is possible. The y-diaphragms are not intended to be used for blocking without the leaves, because their transmission is significantly higher than the leaf transmission (see section 2.3.2). The x-diaphragms have the same maximum velocity as the y-diaphragms. They can be driven back to 20 cm in their half field, but cannot cross the center of the field. They are designed to define the field edges in x-direction and to reduce inter-leaf leakage. The constraints for leaves and diaphragms limit the maximum field size to $40 \times 40 \text{ cm}^2$ and allow fields as far as 12.5 cm offset in y-direction, while the maximum offset in x-direction is not restricted. Notably, the center of a $40 \times 40 \text{ cm}^2$ field lies between two leaves and not in the middle of a central leaf. In figure 2.6, a field formed by leaves and diaphragms is shown schematically. The coordinate system and orientation of this figure is used throughout the rest of this thesis. Y-values increase from left to right, while x-values increase bottom-up. The center of the field is at position $(x = 0; y = 0)$. This nomenclature, though arbitrary, is consistent with the MLC-manual [34] and the aforementioned publication [46].

2.3.2 Performance Characteristics

The performance characteristics of the Elekta MLC are described in the manual [34] and have been investigated by several authors [44, 46, 59]. Furthermore, procedures for quality control of the MLC have been published [43]. In this section, some important features are summarized.

The precision of leaf and diaphragm positioning is 1 mm or better, slightly depending on the gantry angle. The resolution in direction of leaf motion can be chosen as fine as 1 mm, while the resolution perpendicular to leaf motion is 1 cm, defined by the projected

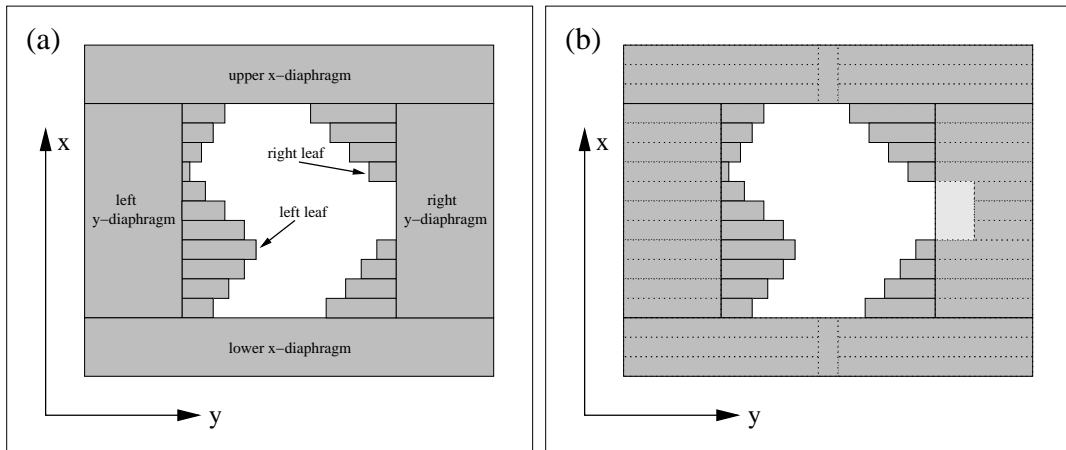


Figure 2.6: Two sketches of the same MLC-field demonstrate the coordinate system and the method of illustration that is used throughout this thesis. (a) illustrates the parts of the MLC seen from BEV. (b) sketches leaves or parts of leaves that are shielded by x- or y-diaphragms with dotted lines. An area that is shielded exclusively by a y-diaphragm is drawn in light grey. In what follows, shielded leaves are only shown if their configuration is important for the illustration.

width of the leaves. At the field edges in x-direction, the x-diaphragms can be positioned so that they do not align with the leaf edges and thus create a local resolution of 1 mm. The mean transmission of the leaves is always smaller than 2%, while the maximum transmission due to inter-leaf leakage is smaller than 5%. The x-diaphragms have a transmission smaller than 1% and published values for the y-diaphragms are about 10% [46]. Any combination of leaves and diaphragms results in a transmission smaller than 0.6%. The 80-20% penumbra for a combination of leaves and y-diaphragm is about 7 mm in water in a depth of 1.6 cm, and up to a few millimeters larger for leaves without diaphragms, if the penumbra is measured perpendicular to the isodose lines. These values increase slightly with increasing photon energy [46].

2.4 Other Types of Multileaf Collimators

Several other companies offer MLCs, but Varian and Siemens are the most important vendors beside Elekta. A summary of the characteristics of these MLCs is given in [84]. MLCs may among other things be classified with respect to typical MLC restrictions like minimum gap, maximum overtravel and interdigitation constraint. Varian MLCs consist of 26 or 40 pairs of leaves with an isocentric leaf width of 1 cm. Like the Elekta MLC, they are focused in x-direction and have curved leaf-ends in y-direction. The leaves can be drawn back for 20 cm in their half field and can overtravel 16 cm, thus defining a maximum field size of 40 x 26 cm² respectively 40 x 40 cm². The design of the leaf sides is different

from that of the Elekta MLC, but also intended to reduce inter-leaf leakage. Varian MLCs allow closing of opposite leaf pairs and opposite adjacent leaves can pass each other. The Siemens MLC consists of 27 inner pairs of leaves with an isocentric leaf width of 1 cm and 2 outer pairs of leaves with a width of 6.5 cm. In this way, the maximum field size is $40 \times 40 \text{ cm}^2$, but only $40 \times 27 \text{ cm}^2$ with the inner leaves. The leaves can be drawn back for 20 cm and can overtravel 10 cm. In contrast to the Elekta or the Varian MLC, the center of the field is shielded by a central leaf pair. Again, the leaf sides are designed to prevent inter-leaf leakage. Opposite leaves are able to close, but opposite adjacent leaves cannot pass each other. The Siemens MLC is focused in x- and y-direction, so that a curved design of the leaf ends is not necessary.

Conformal radiotherapy with a conventional MLC with an isocentric leaf width of usually 1 cm is often not satisfactory for small tumors in close proximity to OARs, e.g. for brain tumors. Specifically for such treatments, *micro multileaf collimators* (mMLCs) with a smaller isocentric leaf width of 1.6-5.0 mm and a maximum field size equal to or less than $10 \times 10 \text{ cm}^2$ have been developed during the last years [57,62,82]. However, an mMLC with a maximum field size of $20 \times 20 \text{ cm}^2$ has been designed as a prototype recently [60].

Furthermore, there is research to develop new kinds of multileaf collimators, which eliminate some of the disadvantages of the state-of-the-art MLCs. At present, some new designs exist only as constructional drawings, while others have already been built as prototypes. The concept of them all is to introduce a new degree of freedom at the cost of a more complicated design. Greer and van Doorn proposed two vertically displaced leaf banks with leaves that can also move laterally to some degree [40]. The intention of this MLC is to reduce the transmission between the leaves as well as to allow a finer resolution perpendicular to leaf motion. Williams and Cooper suggest to attach another collimator below the conventional MLC [80]. A displacement between both collimators leads to a finer resolution perpendicular to leaf motion, too. In contrast to the mMLC, this MLC allows a very fine resolution and a large maximum field size in combination. Webb proposed a design for a shuttling MLC, which consists of two vertically shifted rows of several small attenuating elements that can be moved independently to some extent [77]. Treatments with this kind of MLC have a higher monitor units efficiency than treatments with a conventional MLC.

Chapter 3

Intensity-Modulated Radiotherapy with an MLC

Intensity-modulated radiotherapy is an extension of conformal radiotherapy. While the latter conforms the geometry of the radiation field to the shape of the PTV, IMRT additionally modulates the fluence weight within the radiation field. Fluence weight modulations can be used to either deliver higher tumor doses without increased risk for OARs, or reduce doses to OARs without compromising the treatment of the tumor. In particular, IMRT offers the possibility to create concave dose distributions, which are required to adequately treat certain tumors, e.g. carcinomas of the prostate that wrap around the rectum [78].

As an IMRT treatment handles numerous additional parameters compared to conventional or conformal radiotherapy, the introduction of IMRT is accompanied by new concepts of treatment planning. Conventional and conformal radiotherapy typically use forward planning, which starts with the definition of photon fields to treat the tumor and evaluates the resulting dose distribution afterwards [75]. A more sophisticated concept is inverse planning, where the desired dose distribution is characterized in advance and the fluence weight modulation of the photon fields to deliver such a dose distribution is calculated subsequently [14]. Inverse planning usually approximates the desired dose distribution as closely as possible by optimizing quasi-continuous fluence weight profiles with an iterative optimization algorithm which minimizes an *objective function*. The latter reflects the desired dose distribution through dose restrictions for tumor and OARs. There are numerous possibilities to define the objective function with physical and biological principles [78]. In section 6.1, the objective function of our in-house inverse planning software is presented in detail. Besides, a combination of forward planning and re-optimization of the resulting segments can also be used to plan IMRT [30]. However, inverse planning may be the most suitable strategy for IMRT treatments with complex fluence weight modula-

tions. A detailed history of the development of IMRT and inverse planning can be found elsewhere [75, 78].

The application of IMRT can either be performed with technical devices already in use for conformal radiotherapy like blocks and MLC, or with new and more specialized equipment. In this chapter, several methods to deliver IMRT with an MLC are presented.

3.1 Static Multileaf Collimation

Static multileaf collimation is the IMRT method that forms the subject of this thesis. Since the following chapters discuss the important issues of sMLC in detail, only an overview is given in this section. The sMLC-technique modulates the fluence weight through superimposition of several MLC-segments from the same beam direction. It is a straightforward extension of conformal radiotherapy as it replaces a single segment from each beam incidence by a series of segments. Between two successive segments, the positions of leaves and diaphragms are changed while the beam is off. Static multileaf collimation is also denoted as *step&shoot-technique*, which emphasizes the alternating irradiation-only and movement-only elements.

The quasi-continuous fluence weight profiles of the inverse planning have to be transformed into a series of segments that can be applied with the MLC for sMLC-delivery. This sequencing consists of two major steps. At first, a *clustering algorithm* projects each quasi-continuous profile onto a profile with only a few different fluence weight levels. An example of such a projection is illustrated in figure 3.1. Afterwards, the piecewise constant profile is transformed by a *segmentation algorithm* into a series of segments which restores the clustered profile through superimposition (see figure 3.2). While the example is related to a specific way of sequencing [10], several different *sequencers* have been developed and published during the last years [7, 10, 26, 27, 39, 49, 61, 65, 81, 83]. Further information about their individual characteristics are given in the following chapters.

The transformation of an optimized fluence weight profile into a series of segments modifies the initial profile. The standard way of sequencing uses modifications that are driven by functions of fluence weight, e.g. by minimizing the root mean squared deviation between optimized and clustered profile. As minor modifications of the fluence weight profiles of different beams may interact and lead to major changes of the resulting dose distribution, the deviations introduced by the sequencing are not controlled with respect to dose-based criteria. It is indispensable to control and possibly compensate the sequencing-related modifications of the dose distribution by incorporating the sequencing into the optimization of the dose distribution. There are two major ways to achieve this. Firstly, one can incorporate the sequencing into the optimization from the beginning on [47]. Secondly, it is possible to use an additional step after initial optimization and

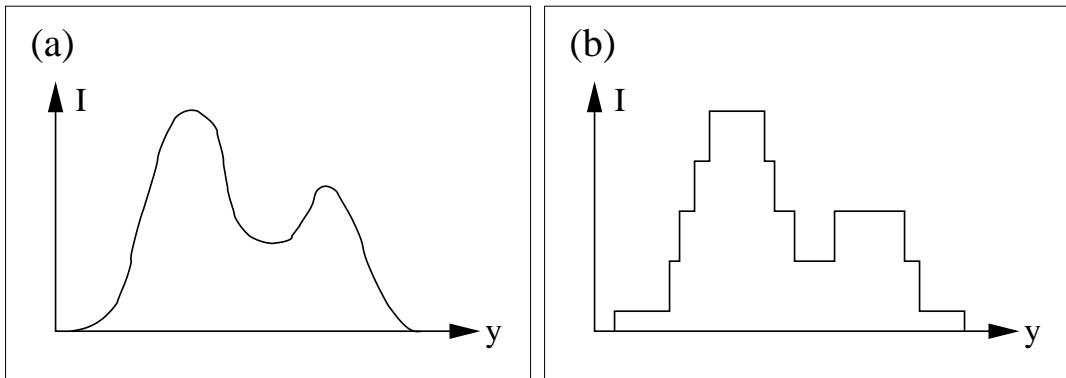


Figure 3.1: Example for the projection of an 1D fluence weight profile (a) onto a clustered profile with five equidistant fluence weight steps (b). The extension to two dimensions is straightforward, because clustering algorithms are typically independent of dimensions.

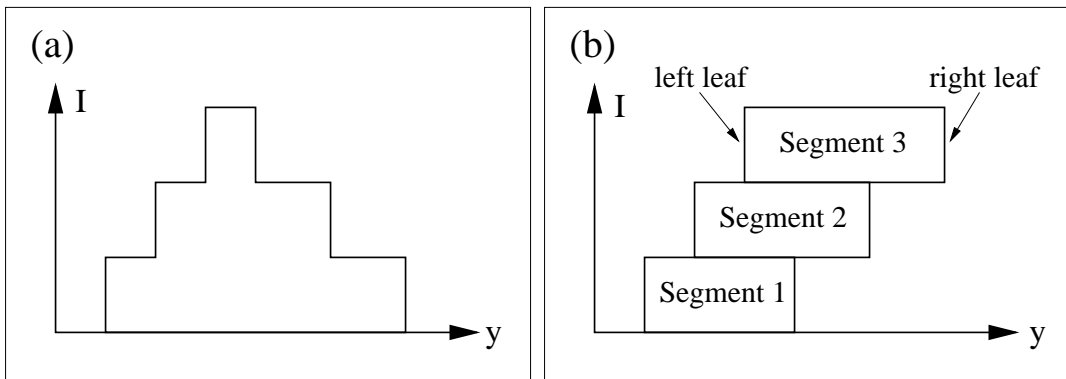


Figure 3.2: Example for the transformation of an 1D clustered profile with three fluence weight levels (a) into a series of three segments (b), each of them defined by a left and a right leaf position. Segmentation for 2D profiles is performed similarly, although modifications due to e.g. the interdigitation constraint may occur (see chapter 5).

sequencing, which re-optimizes the weights and shapes of the segments with respect to the dose distribution [4]. More details about sequencing with dose-based criteria are given in chapters 6 and 7.

One potential drawback of IMRT with the sMLC-technique from a practical point of view is the increased number of segments. As a consequence, segments for sMLC are on average smaller and have less monitor units. There are likely some very small segments and some with only a few monitor units, others may share both characteristics. Therefore, the accuracy of the application of small fields and few monitor units is a major issue for the sMLC-technique [42, 64]. The increased number of segments also raises the issue of leakage through leaves and diaphragms, because the total number of monitor units increases [51]. Furthermore, the start-up behaviour of the linear accelerator becomes crucial, because the

irradiation has to be interrupted and re-started for each segment [16]. The irradiation time of the sMLC-technique is determined by the number of segments, the number of monitor units per segment, the start-up-behaviour and the velocity of leaf positioning. Therefore, it is on average prolonged compared to conformal radiotherapy. The complex issue of minimizing the irradiation time is often seen as a major aim of the sequencing and is further discussed in the following chapters.

Static multileaf collimation introduces a new dosimetric issue. If there are several segments from the same beam incidence, there may be segments adjacent to each other which have a common field edge parallel or perpendicular to leaf motion, as illustrated in figure 3.3. If both segments have equal monitor units, the irradiation of both segments should ideally result in the same dose distribution as for a single segment with the combined area. However, underdosage of parallel matchlines and under- or overdosage of perpendicular matchlines occurs due to the design of the stepped leaf sides and the rounded leaf ends. The stepped leaf sides prevent direct irradiation of the matchlines, because either one or the other leaf side is within the beam. As a consequence, underdosage of the matchline results [69]. The stepped sides are denoted as *tongue&groove-design* and the effect of underdosage of matchlines parallel to leaf motion as *tongue&groove-effect*. The amount of under- or overdosage of the perpendicular matchlines depends on the specific MLC-settings, which determine the exact positions of left and right leaf ends for a desired segment. Sequencing algorithms should take these effects adequately into account to prevent significant under- or overdosage in the relevant regions.

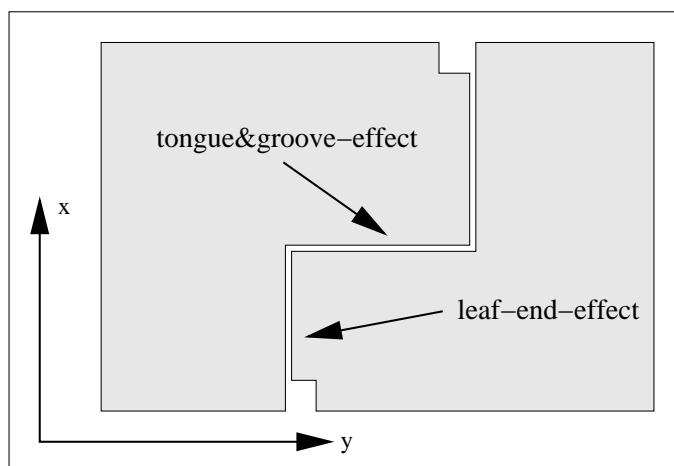


Figure 3.3: Example for different matchlines between two segments, which are illustrated in light gray. The characteristics of matchlines perpendicular to the direction of leaf motion are determined by the rounded leaf ends, parallel to leaf motion, underdosage due to the tongue&groove-design occurs.

The concepts for quality assurance of sMLC-treatments are in principle quite similar to those of conformal radiotherapy, as apart from the issue of matchlines hardly any new features are introduced. However, IMRT treatments with numerous segments are more sensitive regarding systematic and random delivery errors. Therefore, precise quality assurance is essential for sMLC [42].

During the last few years, sMLC has become one of the important methods to deliver IMRT clinically [30, 36]. Numerous institutions prefer to introduce IMRT treatments by sMLC, because it is a rather simple and straightforward extension of routinely-applied conformal radiotherapy. Furthermore, sMLC is completely based on conventional accelerators and MLCs with no need for additional equipment.

3.2 Dynamic Multileaf Collimation

Dynamic Multileaf Collimation (dMLC) modulates the fluence weight by moving the leaves while the irradiation is on. Different irradiation durations for different positions within the field result in local fluence weight modulations. As field shapes change dynamically during continuous irradiation, dMLC is not an extension of conformal radiotherapy like sMLC, but a new concept of radiotherapy.

To deliver an optimized fluence weight profile by means of dMLC, time-dependent leaf and diaphragm positions have to be determined. A single left and right leaf are relevant for the application of the 1D profile in figure 3.4 a. In this example, it is assumed that both leaves move uni-directionally from left to right, starting from the same position on the left edge of the profile. Furthermore, leaf leakage and scatter are neglected. A position y within the field is irradiated during the time interval where the end of the right leaf has already passed this position, while the end of the left leaf has not. If one defines $T_l(y)$ and $T_r(y)$ as the times when the ends of left and right leaf are at position y , then $\Delta T(y) = T_l(y) - T_r(y)$ is the time position y is irradiated. A given fluence weight profile determines $\Delta T(y)$, but not the absolute value of $T_l(y)$ and $T_r(y)$. The remaining degree of freedom can be exploited to minimize the total irradiation time subject to a maximum leaf speed constraint. The solution with minimum time need uses maximum leaf speed of the left leaf for decreasing intervals of the profile and maximum leaf speed of the right leaf for increasing intervals [66–68]. Figure 3.4 b illustrates the solution for the 1D profile. The maximum leaf speed determines the minimum gradient dT/dy for left and right leaf trajectories and is crucial for the irradiation time.

In practice, the 1D solution for a single leaf pair has to be extended for 2D fluence weight profiles. In 2D, left and right leaf positions $T_l^i(y)$ and $T_r^i(y)$ have to be determined for every leaf pair i under consideration of the MLC restrictions. In a first step, the trajectories of every leaf pair are calculated similar to the 1D solution. Secondly,

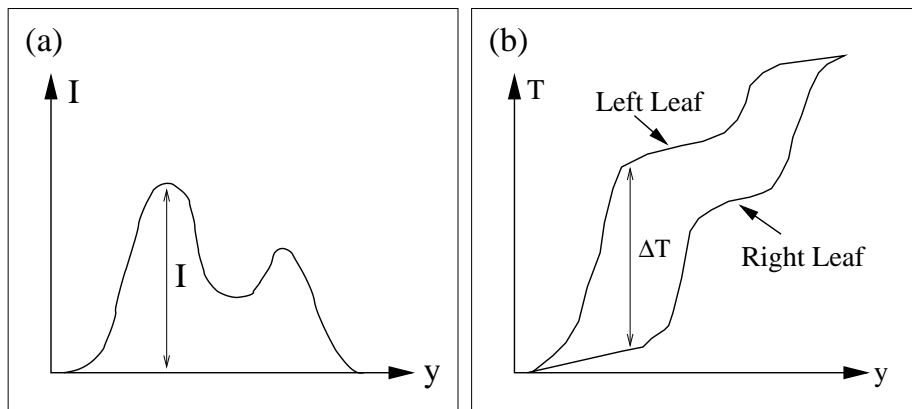


Figure 3.4: Example for the transformation of an 1D fluence weight profile (a) into left and right leaf positions (b). The vertical distance ΔT between left and right leaf trajectory at any position y equals the intensity $I(y)$. 2D solutions have to synchronize adjacent leaf pairs due to the MLC constraints (see text).

adjustments of the trajectories, often denoted as *synchronization*, may be necessary if e.g. the interdigitation constraint is violated by adjacent leaf pairs at any position within the field. Synchronization is performed by reducing the speed of one or more leaves. As a consequence, the irradiation time may increase. More details about the calculation of leaf trajectories for dMLC can be found elsewhere [78].

One should bear in mind that the translation of a continuous fluence weight profile into leaf trajectories is also an approximation, as the leaf velocity is not continuously changing, but piecewise constant. As an example, figure 3.5 illustrates how a continuous profile may be approximated by a profile suitable for dMLC delivery with a few *control points*, which determine the positions where the leaf velocities are changed. The approximation of a continuous profile by dMLC is in most cases more precise than by sMLC for an equal number of control points respectively fluence weight levels, because the approximation of fluence weight gradients is easier for dMLC.

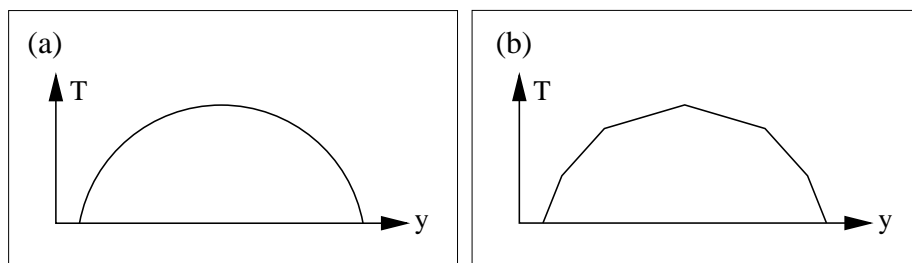


Figure 3.5: Example for the approximation of an 1D fluence weight profile (a) by 7 control points for dMLC delivery (b). More details about this procedure can be found elsewhere [15].

A variety of dMLC algorithms have been published [18, 23, 26, 32, 41, 48, 53, 66–68, 88]. Most of them use the *sliding-window-technique*, where all leaves move uni-directionally for the sake of simplicity. Alternatively, the *close-in-technique* allows leaf-movement in both directions, which is more efficient for the delivery of single fluence weight peaks within the field. The dMLC algorithms mainly differ by how they incorporate the MLC constraints and how they deal with scatter and leaf transmission. The consideration of these effects for the transformation of the profiles into leaf trajectories is necessary to avoid deterioration of the dose distribution.

The start-up behaviour of the linear accelerator is of less concern for the dMLC-technique, because it uses continuous irradiation without any interrupts. Similar to sMLC, leakage and transmission through the leaves are crucial, as the amount of small fields and the total number of monitor units is increased compared to conformal radiotherapy. The application of dMLC is generally more time-efficient than sMLC, because continuous irradiation avoids loss of time due to repeated beam-start-up procedures. The tongue&groove-effect occurs if adjacent leaf pairs irradiate a position y at different moments in time. By synchronization of the leaves, the effect can be eliminated at the cost of slowing down the leaves and thus increasing the irradiation time and the total number of monitor units [72, 79]. In contrast to sMLC, there seems to be general agreement to eliminate the tongue&groove-effect for dMLC applications. Like static multileaf collimation, dMLC is sensitive against systematic and random delivery errors and precise quality assurance is very important for the clinical application. Furthermore, dMLC introduces the quality control of the leaf velocity as a new issue [25].

Dynamic multileaf collimation is the other important application method of IMRT with a conventional MLC [17, 19]. Compared to static multileaf collimation, dMLC is better suited to precisely approximate optimized fluence weight profiles.

3.3 Intensity-Modulated Arc Therapy

Another technique of delivering IMRT by means of a conventional MLC is *intensity-modulated arc therapy* (IMAT). It combines conventional arc therapy with dynamic multileaf collimation. For IMAT delivery, the gantry is rotating continuously around the patient and the leaves of the MLC are moving while the beam is on [12, 87].

Treatment planning for IMAT approximates an arc of typically 275° by static fields at every 5° . Optimization of the fluence weight profiles is performed for all beams and the resulting profiles are transformed into multiple static fields with equidistant fluence weight steps. Segments with equal fluence weight but different gantry angle are gathered to form an arc. The number of different fluence weight levels determines the minimum number of arcs. Additional arcs are necessary if a fluence weight level from one beam

direction consists of more than one segment. During the delivery of an arc, the irradiation is continuous, the gantry is rotating with constant velocity and the leaves are moving, so that they correspond with the planned leaf positions at every 5° . The IMAT treatment is performed by subsequent delivery of all arcs. In analogy to the other techniques, IMAT has to consider the technical restrictions of the MLC. The maximum leaf velocity restricts the distance leaves can travel during a gantry rotation of 5° , thus limiting either the dose rate of the accelerator or the deviations between the leaf positions of subsequent segments. Gantry angles within an arc without any fluence weight require total blocking of the irradiation. If this is not possible due to e.g. a minimum gap constraint, the arc has to be divided into two partial arcs that spare the part without any fluence weight.

Unlike sMLC or dMLC, IMAT is still in the developing stage and its clinical application is in its infancy [86]. The use of an arc as an approximation of numerous beam directions reduces the complexity of the individual fluence weight profiles and thus the number of fluence weight levels. In this way, IMAT has the potential to reduce the treatment time compared to sMLC or dMLC.

3.4 Tomotherapy

*Tomotherapy*¹ uses a similar concept as IMAT by delivering IMRT through a combination of arc therapy and dMLC. In contrast to IMAT, it does not use a conventional MLC, but a quasi-1D slit aperture, which defines a narrow fan-like radiation field with vanes instead of leaves. The gantry with attached MLC is rotated around the patient while the beam is on and the vanes are moving. In this way, intensity modulation within the narrow aperture is achieved. For the treatment of large tumors, several arcs at different locations of the patient have to be applied to create a 2D intensity modulation. The treatment table is therefore shifted along the patient's longitudinal axis during treatment. Contrary to IMAT, only one arc for a fixed position of the patient is used. There are two concepts to deliver tomotherapy, both are mentioned briefly in what follows.

The first was developed in the early 1990s and since then commercialized by NOMOS [22]. Their quasi-1D MLC is called *multivane intensity-modulating collimator* (MIMiC) and consists of two narrow apertures with 20 small vanes each. The latter can either be within the field in closed position or outside in open position. The width of each vane is 1 cm, while the thickness of the aperture is 0.5-2.0 cm. The latter depends on the version of the MIMiC. In this way, a treatment field of 20 cm width and 1-4 cm height with a resolution of typically 1 cm is created. Intensity modulation is achieved by varying the individual times the vanes are in open or closed position. The approximation of the arcs for treatment planning is performed similar to IMAT (see section 3.3). After irradiation of

¹The name 'tomotherapy' emphasizes the analogy to computed tomography (CT).

a single arc, the beam is interrupted and the table is shifted to a new position, so that the next arc irradiates the adjacent region. This procedure is repeated until the whole tumor has been irradiated. A treatment table that can be positioned with a very high accuracy of 0.1-0.2 mm is used in combination with the MIMiC, because inadequate table positioning may introduce serious under- or overdosage at the matchlines between adjacent arcs [21]. Tomotherapy with a MIMiC has found widespread application and is the third important technique for delivering IMRT clinically [20, 70, 73]. Unlike both other methods, it requires specific equipment which is usually not used for conventional or conformal radiotherapy.

A second technique of delivering tomotherapy was proposed in 1993 and has since then been further developed for a prototype system at the University of Wisconsin [55, 56]. In contrast to the first method, the table is not shifted after each arc while the beam is off, but continuously moved during the irradiation of the arcs. In this way, the method is in close analogy to spiral CT-scanning and often denoted as *helical tomotherapy*. The MLC consists of a single slice with 64 vanes of 6.2 mm width and a total field width of 40 cm. So far, no patients have been treated with helical tomotherapy, but the clinical introduction at the University of Wisconsin is under way.

Chapter 4

Clustering

Inverse planning usually results in freely modulated fluence weight profiles, one from every pre-defined beam direction. Each of these quasi-continuous profiles has to be transformed into a series of segments that can be delivered with the MLC. While a precise conversion of a continuous profile would require a very large number of segments, treatment time and number of segments are limited in clinical routine. As a consequence, the complexity of the profiles has to be reduced substantially and the quasi-continuous profiles are projected onto profiles with few fluence weight levels during the clustering.

In the following section, we introduce the conventional way of clustering and demonstrate its shortcomings. Afterwards, a new clustering algorithm is presented, which has been developed to eliminate the drawbacks of the conventional strategy. Finally, we demonstrate the performance of our clustering in comparison to the conventional method for several examples.

4.1 The Bortfeld-Boyer Method of Clustering

At present, most sequencers for sMLC delivery use a clustering algorithm similar to the *Bortfeld-Boyer method*, which was published in [10]. This method projects each quasi-continuous fluence weight profile onto a clustered profile with equidistant fluence weight levels. As a first step, the number of fluence weight levels or the fluence weight step as distance between adjacent levels is specified by the user. Subsequently, the other parameter can be calculated, if one e.g. defines the maximum fluence weight of the profile as product of both parameters. In this way, a fluence weight lattice with the fluence weight step as lattice parameter is determined. Each fluence weight value of the quasi-continuous profile is projected onto the closest fluence weight value on the lattice. To minimize the introduced fluence weight modifications, it is useful to shift the lattice along the fluence weight axis until the difference between quasi-continuous and clustered fluence weight profile in terms

of e.g. root mean squared deviation is minimal. Figure 4.1 shows two examples of this procedure.

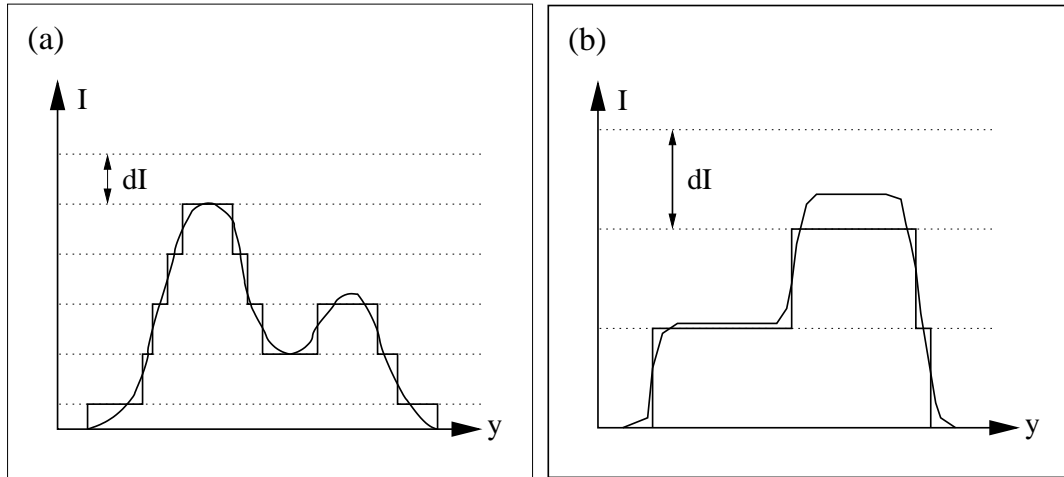


Figure 4.1: Examples for equidistant clustering related to [10] of 1D fluence weight profiles with 5 (a) or 2 levels (b). The approximation with 5 levels shows only minor deviations, while the coarse clustering with 2 levels is insufficient. Notice that the lattice of the clustering with 5 levels is shifted along the fluence weight axis to minimize the deviations between quasi-continuous and clustered profile.

With increasing number of fluence weight levels, the deviations between quasi-continuous and clustered profiles decrease. Generally, it is possible to achieve a rather good approximation with a limited number of levels [35]. However, this may not hold for a coarse approximation with only very few levels, which is desirable to minimize the number of segments respectively the irradiation time. An example of an approximation with only two different fluence weight levels is given in figure 4.1 b. It is evident, that the stipulation of equidistant fluence weight steps can introduce large deviations. Alternatively, one could apply a clustering method with variable fluence weight steps, where the additional degree of freedom to vary the step size can be exploited to improve the approximation of the quasi-continuous fluence weight profile.

4.2 Clustering Algorithm

Starting point of our clustering algorithm are the fluence weight profiles generated by the inverse planning software HYPERION. The quasi-continuous profiles are sampled on a grid of 10 mm according to the leaf width and typically 2 mm in direction of leaf motion. The latter resolution is considered necessary and sufficient for adequate IMRT delivery [9]. Notice that HYPERION considers scatter and leakage during the optimization of the fluence weight profiles and applies a smoothing constraint to reduce their complexity [3]. Further

details about HYPERION are given in section 6.1.

Every quasi-continuous profile is projected onto a piecewise constant profile with few fluence weight levels. A user-defined bandwidth b limits the tolerated difference between quasi-continuous and clustered fluence weight of any element of the profile. The clustering algorithm groups fluence weight elements together to form *clusters*. A cluster is composed of one or more elements of similar fluence weight. The cluster value as common fluence weight is calculated as the mean value of all elements that belong to this cluster. In the beginning, every fluence weight element is a cluster of its own. An element or a whole cluster is added to another cluster if all elements of the resulting new cluster are no more than some ϵ apart from the new cluster value. The initial value of ϵ is $b/16$. If all elements are grouped for $\epsilon = b/16$, multiplication by a constant factor increases ϵ . The factor is chosen so that ϵ equals b after 16 iterations. This procedure of clustering with an iteratively increasing ϵ is repeated until $\epsilon > b$. Alternatively, one can define a certain minimum number of clusters as a criterion for the termination of the clustering. In this case, the algorithm either stops if $\epsilon > b$ or if the number of clusters equals the specified minimum number, whichever occurs first. Finally, the clustered profile is created by replacing the quasi-continuous fluence weight value with the related cluster value for every fluence weight element. The resulting profile strictly satisfies the restriction of a maximum deviation of b between quasi-continuous and clustered value for any fluence weight element. An example for the clustering of a 1D profile is illustrated for two different values of b in figure 4.2. The figure demonstrates the influence of the bandwidth, as increasing b typically worsens the approximation of the quasi-continuous profile, but reduces the number of resulting fluence weight levels. Notice that the algorithm is independent of the position of the fluence weight elements, so 1D and 2D profiles are treated alike.

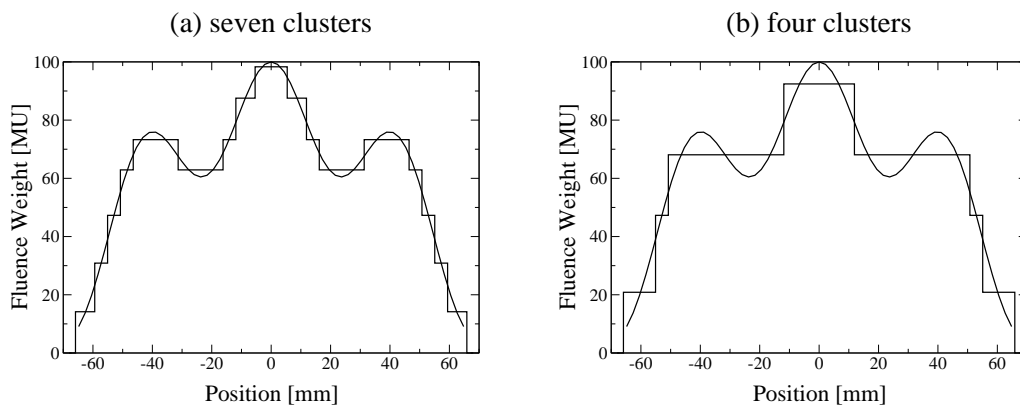


Figure 4.2: Example for the clustering of an 1D profile of the type $z = c_1 x^2 + \cos^2(c_2 |x|) + c_3$, where z denotes the fluence weight, x the position and c_1, c_2, c_3 are constants. A bandwidth b of 10 MU leads to a very close approximation with 7 clusters (a), while $b = 20$ MU results in only 4 clusters and a less complex clustered profile (b).

The algorithm ensures that the deviation of any element is equal to or smaller than b , but not that the difference between different cluster values is equal to or greater than b . Cluster values are never smaller than the minimum fluence weight and never greater than the maximum fluence weight of the quasi-continuous profile. As a consequence, the clustering routine is not able to exclude elements from the fluence weight profile by reducing their values to zero. However, the optimization of the fluence weight profile considers the bandwidth also as a *minimum fluence weight constraint* and guarantees that each fluence weight value of the profile is equal to or greater than b after the optimization. Exclusion of any fluence weight element by the clustering is therefore not required.

4.3 Modifications of the Clustered Profiles

Technical restrictions of the Elekta MLC as described in section 2.3.1 limit the possibilities to shape and position the segments within the radiation field. Further modifications of the clustered profile ensure that the final profile is directly transformable into a series of segments.

The minimum gap constraint limits the minimum segment width in direction of leaf motion. After the clustering, peaks smaller than this may occur and violate this restriction. A routine erases such peaks by associating the fluence weight elements of the peaks to the surrounding cluster. Afterwards, the cluster values are updated to consider the new constellation of clusters. Notice that the maximum fluence weight deviation of elements of the modified clusters may now exceed b . The maximum overtravel constraint limits the position of the segments within the field. Segments which consist exclusively of elements with a distance greater than this constraint offset from the center of the field in direction of leaf motion cannot be delivered with the MLC. A routine extends such isolated peaks in the fluence weight profile towards the center of the field until the violation of the overtravel constraint is eliminated. Again, cluster values are updated and maximum deviations greater than b may result. As those modifications typically either concern only a few fluence weight elements (minimum gap corrections), or occur only rarely (maximum overtravel corrections), the introduced violations of the maximum deviation b is expected to have only minor consequences for the dose distribution. An example for modifications of a clustered profile due to the minimum gap and the maximum overtravel constraint is illustrated in figure 4.3.

It is also possible to apply general constraints beside the technical restrictions. The minimum gap constraint can be replaced by a *minimum segment width constraint*, which guarantees that each segment has a minimum width of at least e.g. 2 cm. Furthermore, a constraint for the minimum distance between two peaks of the clustered profile in direction of leaf motion can be defined. Contrary to the minimum gap constraint, this *minimum*

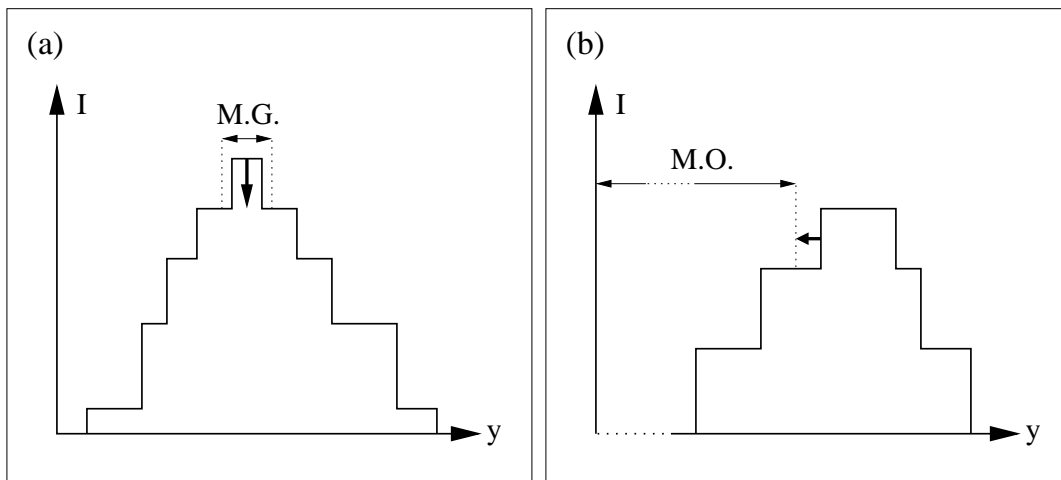


Figure 4.3: Examples for modifications of the clustered profiles to eliminate violations of the minimum gap constraint (a), where the relevant fluence weight peak is erased, and the maximum overtravel constraint (b), where the relevant part of the profile is extended towards the center of the field.

segment separation constraint modifies the profile so that valleys and not peaks are eliminated. These additional constraints are used to reduce the number of segments, to result in more reasonably shaped segments and to eliminate underdosage due to matchlines.

4.4 Performance of the Clustering

In appendix A, the performance of the clustering is investigated in detail. The results are summarized in this section. An implementation of the Elekta MLC with a maximum overtravel constraint of 12.5 cm and 1 cm for minimum gap and interdigitation constraint was used. Clustering was done for 8 mathematical and 2 clinical profiles. As examples, two of the mathematical and both clinical profiles are illustrated in figure 4.4. All profiles are normalized to a maximum fluence weight of 100 MU.

Clustering was performed for three values of the bandwidth. Our method was compared to an extended version of the Bortfeld-Boyer method (see section 4.1 and [10] for the principles of the method and appendix A for details about our specific implementation). We examined the mean squared deviation rms and the maximum deviation max between original and clustered values of the fluence weight elements of the profiles. However, both clustering methods specify the bandwidth respectively the size of the fluence weight step, which both determine the upper limit of max, before the clustering and aim at minimizing rms. In this way, rms is the relevant parameter to compare the performance of both clustering methods.

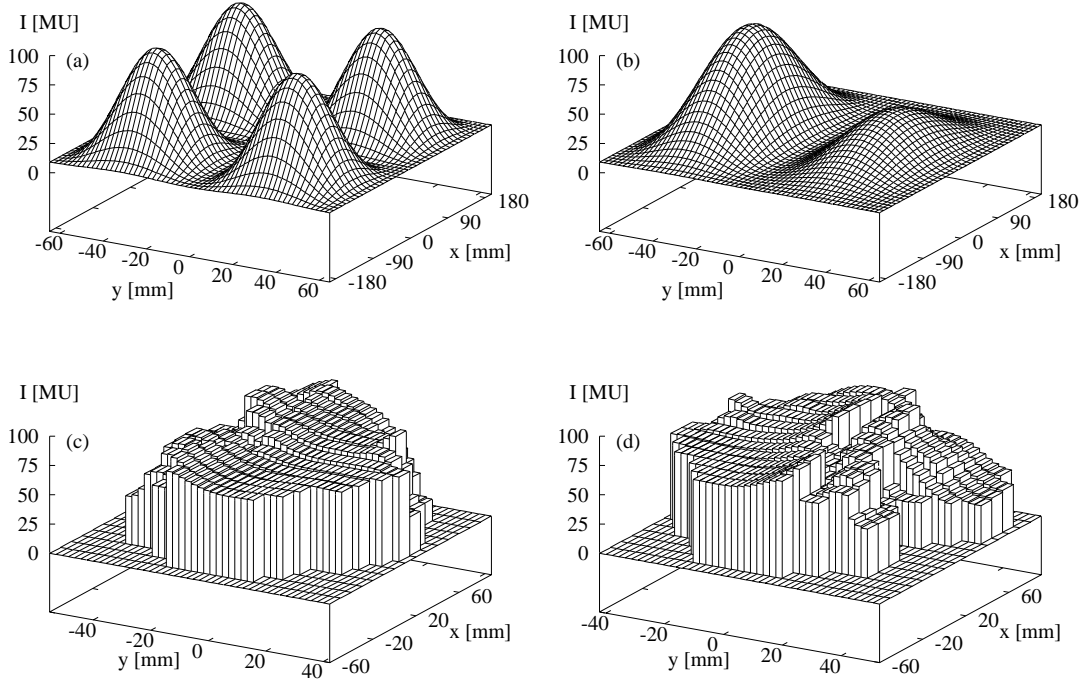


Figure 4.4: Two mathematical and two clinical profiles to test the performance of the sequencer: (a) $z = \sin^2(0.033\pi|y|) \cdot \sin^2(0.05\pi|x|) + \text{const.}$, (b) $z = a_1 \cdot \sin^2(0.033\pi|y|) \cdot \cos^2(0.025\pi|x|) + \text{const.}$ ($a_1 = 7/3 \cdot a_2$), (c) 5-field prostate case, beam from 72° , (d) 5-field prostate case, beam from 288° . Notice that a_1 is used to create the left and a_2 to create the right peak in (b).

In table 4.1, the results are summarized. The presented figures are mean values, which are averaged over the 10 profiles. The mean squared deviation of our clustering is about 10-15% smaller and the maximum deviation about 5-10% larger than those of the Bortfeld-Boyer method.

bandwidth	clusters	rms _{var}	rms _{equ}	max _{var}	max _{equ}
38	2.9	8.8	9.7	22.3	20.9
19	4.2	5.7	6.6	14.1	13.0
9	7.9	3.2	3.8	7.8	7.4

Table 4.1: Results of the clustering for three different values of the bandwidth averaged over the 10 profiles. Listed are the number of clusters, rms and max for our clustering method (labelled as 'var') and for the Bortfeld-Boyer method (labelled as 'equ'). Notice that both methods were restricted to the same number of clusters respectively fluence weight levels. Bandwidth, rms and max have MU as unit.

The results of both clustering methods with seven fluence steps respectively clusters for the 1D profile of section 4.2 are illustrated in figure 4.5. While equidistant clustering is restricted to a lattice with a constant lattice parameter, our method may freely distribute its fluence weight levels to minimize the rms. As a consequence, it approximates the complex central peak with three instead of two and the smaller peaks with 5 instead of 6 levels. In this way, it reduces the rms by 25% compared to equidistant clustering.

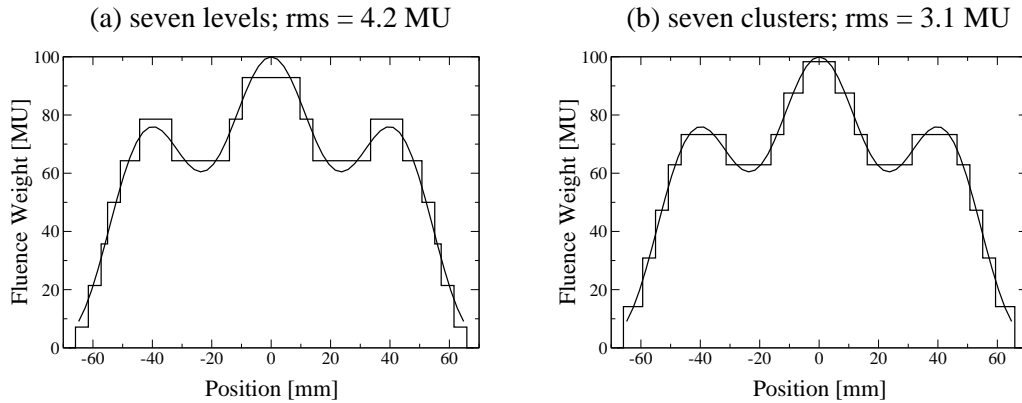


Figure 4.5: Example for the results of the clustering of the 1D profile already presented in section 4.2. Equidistant clustering with a fixed lattice parameter results in an rms of 4.2 MU (a), while our clustering method shifts its fluence weight levels to further reduce the rms by 25% (b).

While no profile violated the maximum overtravel constraint after the clustering, some peaks that violated the minimum gap constraint had to be erased subsequently. In some cases, this increased the rms by up to 100%, the max even stronger (see appendix A). It seems to be likely that a more sophisticated method to eliminate these peaks could lead to better results.

These findings give evidence that clustering with variable instead of uniform fluence weight steps on average improves the conformity between optimized and clustered profile for a fixed number of fluence weight levels. Our results have recently been confirmed by publications of Wu et al. [81] and Beavis et al. [7]. Both developed and tested clustering algorithms with variable fluence weight steps. Wu et al. approximate the continuous fluence weight profiles with a k -means clustering algorithm by minimizing the rms between continuous and clustered profile for a given number of k clusters. Similar to our method, the number of clusters is related to the user-defined maximum deviation between the value of any fluence weight element before and after the clustering. However, their method does not consider the restrictions of the Elekta MLC during the clustering. As a consequence, the clustered profiles may not directly be deliverable as a series of segments and the segmentation may have to introduce modifications of the profiles which are uncontrolled

with respect to fluence weight or dose. The method of Beavis et al. considers every leaf pair independently. The part of the field related to a specific leaf pair is divided into a given number of small areas with variable width in direction of leaf motion. The intensity of each of these areas is determined by the mean value of the elements belonging to it. The method optimizes the widths of the areas by minimizing the rms between the continuous profile and the profile created by the mean intensities of each partial area.

Chapter 5

Segmentation

Several sequencers have been published during the last years [7, 10, 26, 27, 39, 61, 65, 81, 83]. They typically use similar clustering methods, but different segmentation concepts. However, most of the segmentation algorithms aim at either minimizing the number of segments [27, 65, 83] or the total number of monitor units [10]. The number of segments determines the number of beam interrupts. Until recently, the time interval between the irradiation of successive segments was quite large due to technical reasons like slow beam start-up or quality control procedures. The treatment time for sMLC was therefore mainly determined by the number of beam interrupts. Nowadays, the necessary time delay between subsequent segments is only a few seconds for most treatment units. As a consequence, the number of segments is not that crucial any more for the treatment time and IMRT with 50 segments can be delivered in about the same time as conformal treatments [24]. The minimization of the total number of monitor units aims at reducing the amount of leakage as far as possible. Beside these aims, there are other important aspects like the tongue&groove-effect or setup and treatment verification, which influence the quality of an sMLC treatment.

In this chapter, a new segmentation algorithm is presented, which considers multiple issues for the transformation of a clustered profile into a series of segments. A shortened description of the segmentation algorithm can also be found in appendix A. At first, an overview of the concept is given, followed by the description of all important elements of the segmentation. Afterwards, general features of the algorithm are discussed in detail. Finally, we demonstrate the performance of the segmentation for several cases.

5.1 Segmentation Algorithm

5.1.1 Concept

From every beam direction, a clustered profile is segmented into a series of segments. The major steps of transforming a profile into segments are the following:

1. **Preparation:** The clustered profile is transformed into a series of pre-segment shapes, one for every different fluence weight level. Pre-segments can be composed of real segments with the same fluence weight, but may itself not be implementable with the MLC. All constraints and some other parameters are defined.
2. **Segmentation:** If any pre-segment shape is already deliverable with the MLC, it is used as a new segment. Otherwise, it is divided into smaller segment shapes until every shape can be applied with an MLC. After the specification of all segments, leaf and diaphragm positions are calculated for every segment.
3. **Superimposition of Segments:** Due to the method of segmentation, different segments may have identical shape. Such segments are eliminated until every segment shape is unique.
4. **Merging of Segments:** Segments which can be delivered as one field are merged to form a single segment.
5. **Sorting of Segments:** After the segmentation, the resulting segments are sorted for the delivery to e.g. minimize the total amount of leaf travel between subsequent segments.

5.1.2 Preparation

Prior to the segmentation, several parameters have to be defined. The minimum gap, the maximum overtravel and the interdigitation constraint for leaves and diaphragms as well as the number of leaves and the leaf width are determined by the specific MLC. In the examples of the following sections we assume that the minimum gap and the interdigitation constraint have equal values for the sake of simplicity. As mentioned in section 4.2, the typical area of a fluence weight element is $10 \times 2 \text{ mm}^2$. Every clustered profile has to satisfy the technical restrictions of the MLC (see section 4.3). At first, it is transformed into a series of pre-segments. Therefore, a horizontal projection of the profile at every different fluence weight value is used as a pre-segment shape. An example of this procedure is illustrated in figure 5.1. This first guess of the segments is the lower limit of the number of segments, because every fluence weight level is transformed into a single segment

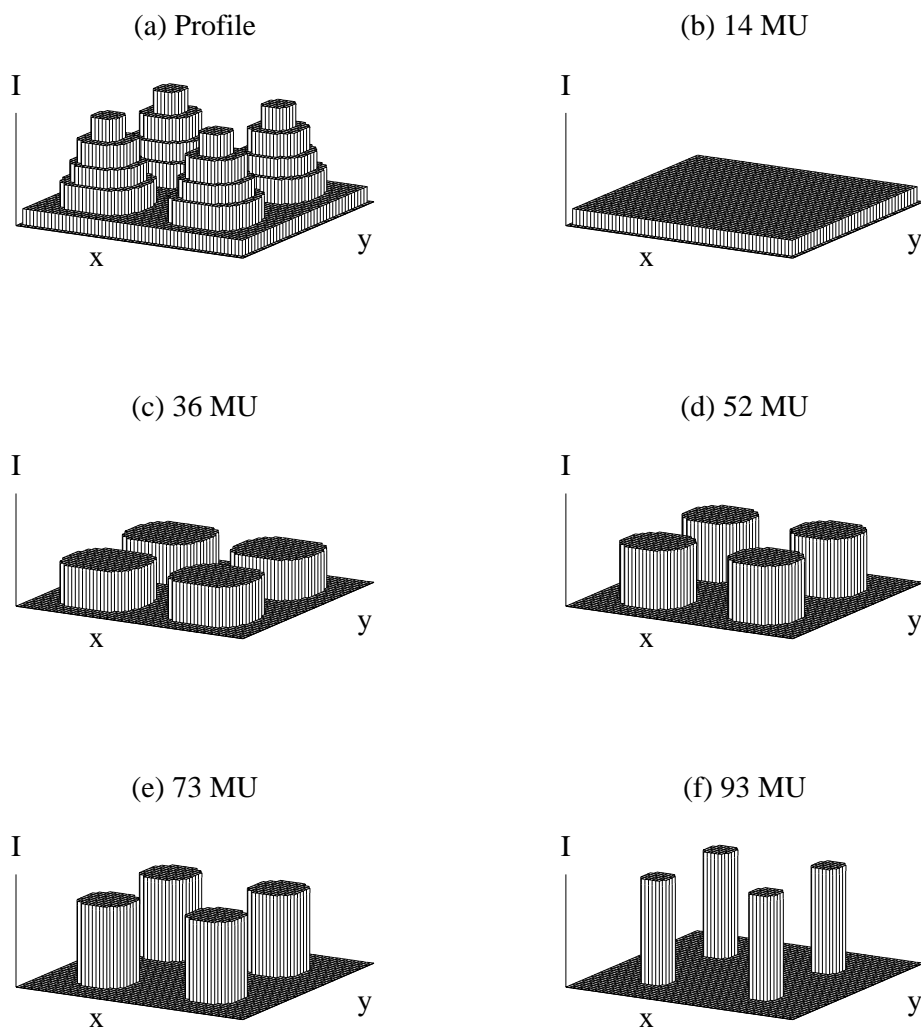


Figure 5.1: Example for the transformation of a clustered profile with five fluence weight levels (a) into a series of five pre-segments (b-f). Each different fluence weight level results in a single pre-segment with the related number of monitor units. Afterwards, the monitor units are modified as described in the text.

only. However, the pre-segments may still violate the constraints and may thus not be implementable with the MLC.

In the beginning, the minimum number of monitor units of any element belonging to a pre-segment is attributed to the pre-segment as monitor units (see figure 5.1). Afterwards, the number of monitor units of every pre-segment is updated to the difference between its current value and the next lower value. In this way, superimposition of the pre-segments with related monitor units exactly reproduces the clustered profile.

5.1.3 Segmentation

If a pre-segment is not deliverable with the MLC, it is divided into a series of smaller segments. The segmentation starts in the lower left corner of such segments. The lowest row of the first segment consists of the lower left element and all elements to the right in direct connection with it. Other elements in this row which are separated from these elements by an area of zero fluence weight are not considered. In the next step, the adjacent row above is examined. If there are elements in direct connection to the chosen elements below, they are considered for inclusion with the first segment. If they all belong to the same area and are not separated from each other by regions of zero fluence weight, they are added to the segment. Otherwise, only the elements that belong to the first region to the left are added. Afterwards, the adjacent row above is considered. The described procedure is repeated until the segment cannot be enlarged further. This is the case if the upper field border is reached or no elements from the current row can be added to the segment. The latter occurs if either there are no elements with any fluence weight in the current row or if the elements would introduce a violation of the interdigitation constraint in combination with the already chosen elements of the adjacent row below. In the next step, all elements that form the first segment are eliminated from the pre-segment. The segmentation as described above is continued with the remaining part of the pre-segment to find the second segment and so on. The segmentation is finished if the pre-segment has been completely transformed into a series of segments. An example of the procedure is illustrated in figure 5.2.

The segmentation algorithm as described above may in some cases result in a series of segments with insufficient shape. An example for such a situation is illustrated in figure 5.3, where the pre-segment is divided into three segments, one of them large, the others small. Another possibility, which leads to only two segments of almost equal size, is also demonstrated. As a consequence of these findings, an improved concept to determine the segment shapes has been incorporated into the segmentation algorithm. The idea behind it is to reduce the size of an initially found segment, if the remaining segment would have an insufficient shape. Such situations may occur, if the conventional segmentation algorithm splits the pre-segment with horizontal cuts. As a consequence, the remaining segment may consist of several small regions separate from each other as shown in figure 5.3 b. The extended segmentation algorithm prevents such situations by replacing horizontal cuts by vertical ones if possible (see figure 5.3 c). However, a vertical cut may introduce a violation of minimum gap, interdigitation or maximum overtravel constraint. Therefore, vertical cuts are only used to replace horizontal ones, if they do not cause any of such violations. The situations where these modifications of the segment shape occur can be quite complex and at multiple locations. Segments may thus have several vertical and horizontal borders towards each other.

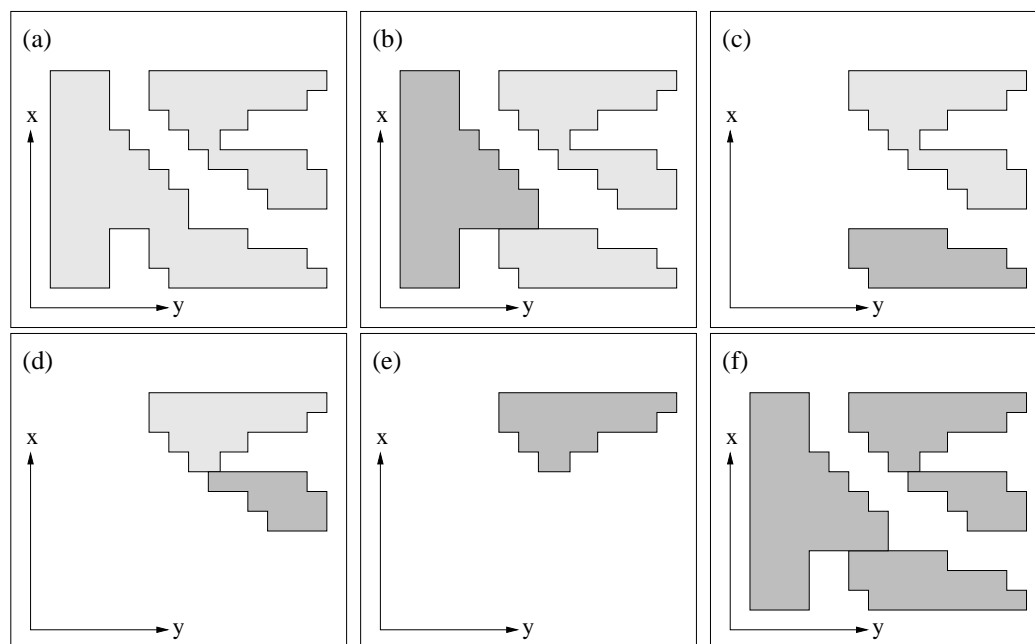


Figure 5.2: Example for the segmentation of a pre-segment (illustrated in (a) in light gray) into a series of segments (illustrated in (b-f) in dark grey). The pre-segment is split if it consists of areas which are separated from each other by regions of zero fluence weight in direction of leaf motion (b), if it contains regions that have no direct connection to each other at all (c), or if adjacent rows of the segment violate the interdigitation constraint (d). The resulting segments re-establish the pre-segment through superimposition (f).

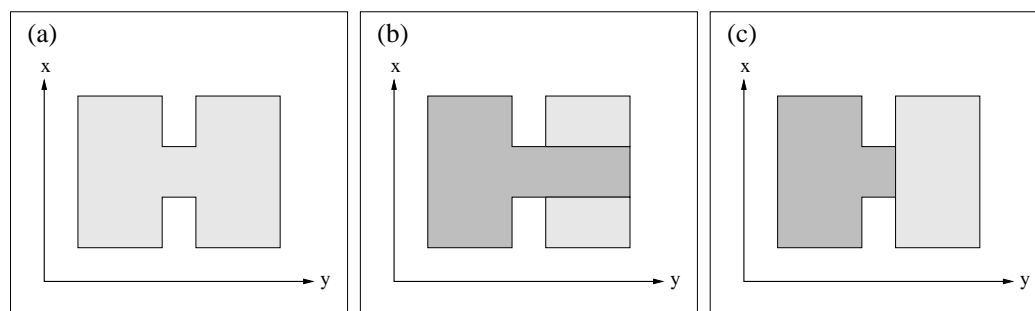


Figure 5.3: Example for a situation where the conventional segmentation of a pre-segment (illustrated in (a) in light gray) leads to three unsatisfactory segments (b). An improved method of segmentation results in only two reasonably shaped segments (c).

At this stage, some segments may still not be deliverable with an Elekta MLC. Such situations occur if segments are offset from the center of the field in vertical direction, e.g. if a segment is located exclusively in one half field as illustrated in figure 5.4 a. In this case, the lower half field is shielded by the lower x-diaphragm. As this diaphragm cannot pass the center of the field, it is difficult to shield the area between the center of the field and the

lower border of the segment. Due to the minimum gap constraint, leaves cannot completely close. A thin area referred to as *flagpole* between the lower border of the segment and the center of the field is thus exposed to unwanted irradiation (see figure 5.4 b). This solution is not satisfactory, because the area to be irradiated additionally may be quite large, if the segment is far offset from the center of the field. Our algorithm modifies this strategy by moving the gap between opposite leaves under one of the y-diaphragms. The thin area is thus not exposed to direct irradiation any more, but shielded by the relevant y-diaphragm. In this case, an adjacent leaf that aligns with the y-diaphragm has to be drawn back to satisfy the interdigitation constraint, thus increasing the area that is shielded exclusively by the y-diaphragm (see figure 5.4 c). In this way, the strategy replaces the fully irradiated flagpole by a slightly larger shielded area with increased transmission.

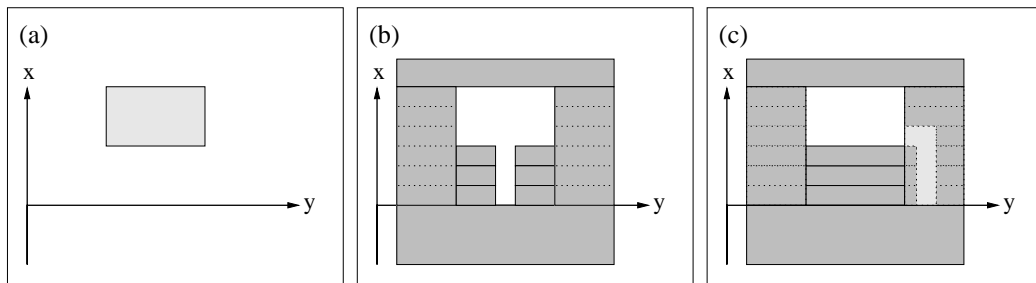


Figure 5.4: Example for a segment (illustrated in (a) in light gray) offset from the center of the field in the upper half field. A straightforward strategy for the positioning of leaves and diaphragms adds an additional area to be irradiated to the segment to satisfy the minimum gap constraint (b). Alternatively, the gap between opposing leaves can be moved under one of the y-diaphragms (c). Notice that the area shown in light gray in (c) is only shielded by the right y-diaphragm.

In some cases, this method cannot be used (see figure 5.5). In this example, the leaves between the center of the field and the lower border of the segment can neither be moved under left nor right y-diaphragm due to the interdigitation constraint. In contrast to the example of figure 5.4, the adjacent left or right leaf cannot be drawn back, because it shields an area which is not additionally shielded by a y-diaphragm. In such a situation, the segment has to be split into smaller segments. The algorithm splits the segment by a vertical cut if this does not introduce a violation of the minimum gap constraint for any of the two new segments. Otherwise, the segment is split by a horizontal cut, so that at least the resulting segment next to the center of the field is implementable. Eventually, the other segment has to be further split into smaller ones. Figure 5.5 shows an example of such a procedure for a segment vertically offset from the center of the field.

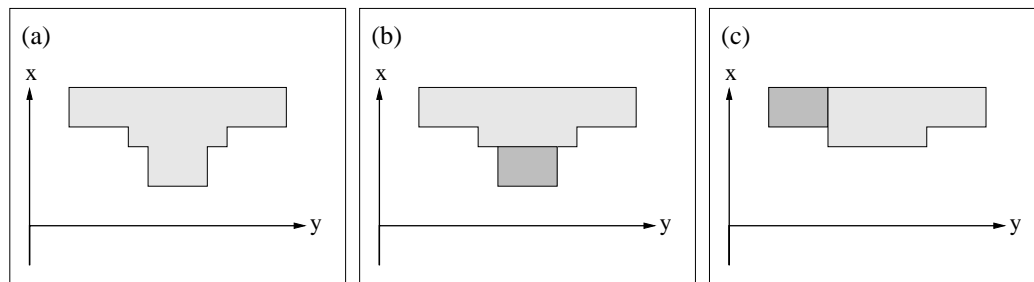


Figure 5.5: Example for a segment (illustrated in (a) in light gray) offset from the center of the field in the upper half field which has to be split into smaller segments. At first, a horizontal cut is performed (b), because a vertical one would introduce a violation of the minimum gap constraint for one of the resulting segments. The upper segment is further split by a horizontal cut (c). In the end, the pre-segment has been transformed into three implementable segments.

After these modifications, the pre-segment has been transformed into segments which are all deliverable with the MLC. Superimposition exactly reproduces the pre-segment. The number of monitor units related to the pre-segment is attributed to all the resulting segments.

5.1.4 Leaf Positions

After the series of segments has been found by defining the segment shapes as described in the previous section, leaf and diaphragm positions are calculated. The segmentation procedure guarantees that all segments are implementable and that it is possible to specify valid leaf and diaphragm positions. This procedure is described in what follows and illustrated for some examples in figure 5.6.

At first, the positions of x- and y-diaphragms are determined to define the maximum field dimensions in every direction. Afterwards, left and right leaves are positioned to specify the left and right field edges. Leaf pairs outside the field which are shielded by x-diaphragms are positioned at the center of the field with a distance of the minimum gap constraint between them.

If a segment is exclusively in the upper or the lower half field, the x-diaphragm of the other half field is moved to the center of the field to shield its half field completely. The left and right leaves between the center of the field and the segment border next to the center are all moved either under the left or the right y-diaphragm (see also section 5.1.3). In some cases, movement is only possible under one of the y-diaphragms due to the interdigitation constraint. If both y-diaphragms are able to shield the leaves, the side where the y-diaphragm is closer to the center of the field is chosen. Opposite leaves are positioned under the y-diaphragm with a distance of the minimum gap constraint between

them. A pre-defined overlap of typically 5 mm is maintained between the y-diaphragm and the opposing leaves to reduce leakage due to scattered photons. Eventually, the use of an overlap may not be implementable due to the maximum overtravel constraint. In this case, y-diaphragm and opposing leaves are moved to the same position.

A segment may consist of two or more vertically separated regions to be irradiated, either due to merging of segments (see section 5.1.6 below) or if a pre-segment with such characteristics is already implementable with the MLC. The area between two separate regions is shielded by a combination of leaves and y-diaphragms in analogy to the aforementioned strategy of leaf positioning for segments which are exclusively in the lower or upper half field. Notice that the situation for areas to be shielded between two regions to be irradiated is more complex, because both upper and lower adjacent leaf positions have to be considered for the decision, under which y-diaphragm the relevant leaf pairs can be moved. More details about such segments and their leaf positioning is given in section 5.1.6.

Finally, it may be necessary to modify the leaf positions at horizontal borders between regions that are irradiated and those that are shielded due to a violation of the interdigitation constraint. If this is the case, a shielded leaf is drawn back so that it maintains a distance of the interdigitation constraint towards the adjacent opposing leaf, similar to the procedure already described in section 5.1.3.

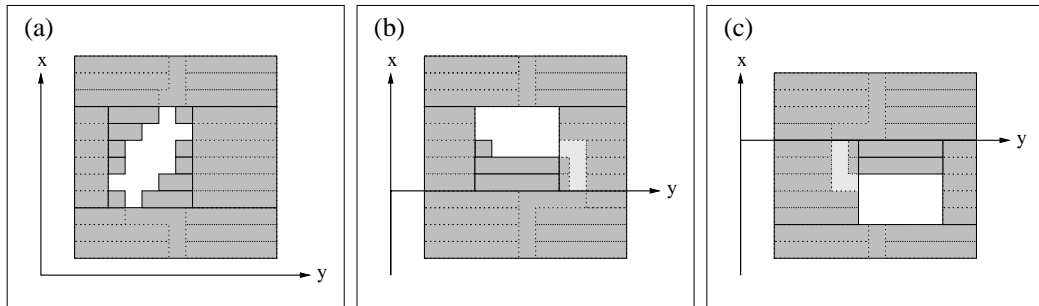


Figure 5.6: Examples for the leaf positioning. Leaf positions outside but adjacent to the field have to be drawn back to satisfy the interdigitation constraint (a). Some leaves have to be moved under the opposite y-diaphragm for a segment that is exclusively in the upper (b) or in the lower half field (c). Notice that the relevant leaves are moved under the left and not the right y-diaphragm in (c), because the left y-diaphragm is closer to the center of the field.

5.1.5 Superimposition of Segments

If the segmentation of all optimized fluence weight profiles into series of segments has been finished, segments may have identical shape. This may be the case, if e.g. a large peak in the clustered profile results in several segments with different number of monitor

units, but equal shape. If such segments exist, the algorithm eliminates all but one of them, so that the segment shape is unique afterwards. The sum of the monitor units of all identically shaped segments is attributed to the remaining segment. An example for the superimposition and the following elimination of segments is illustrated in figure 5.7.

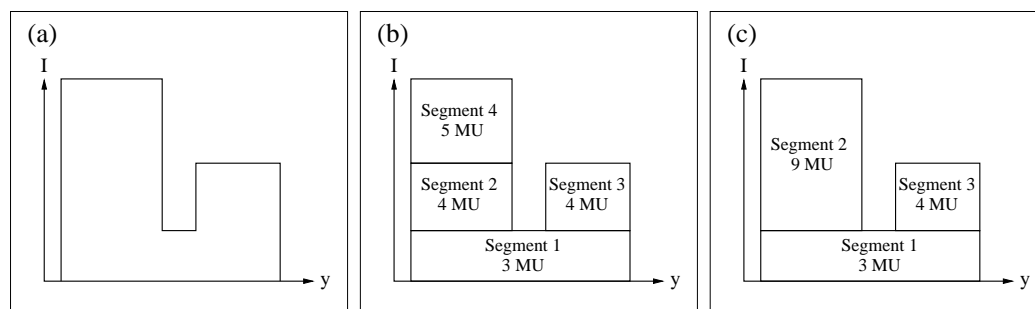


Figure 5.7: Example for the segmentation and superimposition of an 1D profile with three fluence weight levels (a). At first, the profile is divided into three pre-segments which result in four segments after the segmentation (b). As the second and the fourth segment have identical shape, the latter is eliminated and the second segment is attributed to the sum of the monitor units of both segments.

5.1.6 Merging of Segments

The remaining segments typically consist of a single region to be irradiated. However, multiple regions may also be deliverable with the MLC as a single segment. The algorithm examines combinations of the set of segments. If such a combination of segments is deliverable, the segments are merged to form a new segment. Necessarily, segments can only be merged, if they have an equal number of monitor units, as otherwise the correspondence with the clustered profile would be destroyed.

The algorithm considers all segments that have equal monitor units and do not have fluence weight elements in common. If some of those segments can be implemented simultaneously, they are merged to form a new segment and the constituents are deleted from the list of segments. Afterwards, leaf positions for the new segment are calculated as described in section 5.1.4. In many cases, the new segment may not be deliverable. This may either be the case if the two segments to be merged are separated from each other in direction of leaf motion, or if the leaf positioning for the composite segment is not possible without violation of the interdigitation constraint. In such situations, merging of the segments is not performed.

The necessary conditions for successfully merging of two vertically displaced segments can be specified in a general way. It is required that both segments have either common left or right y -diaphragm position. Otherwise, shielding of the intermediate region by moving

leaves under one of the y-diaphragms is not possible due to the interdigitation constraint. Examples of several situations where merging of two segments is either possible or not are illustrated in figure 5.8.

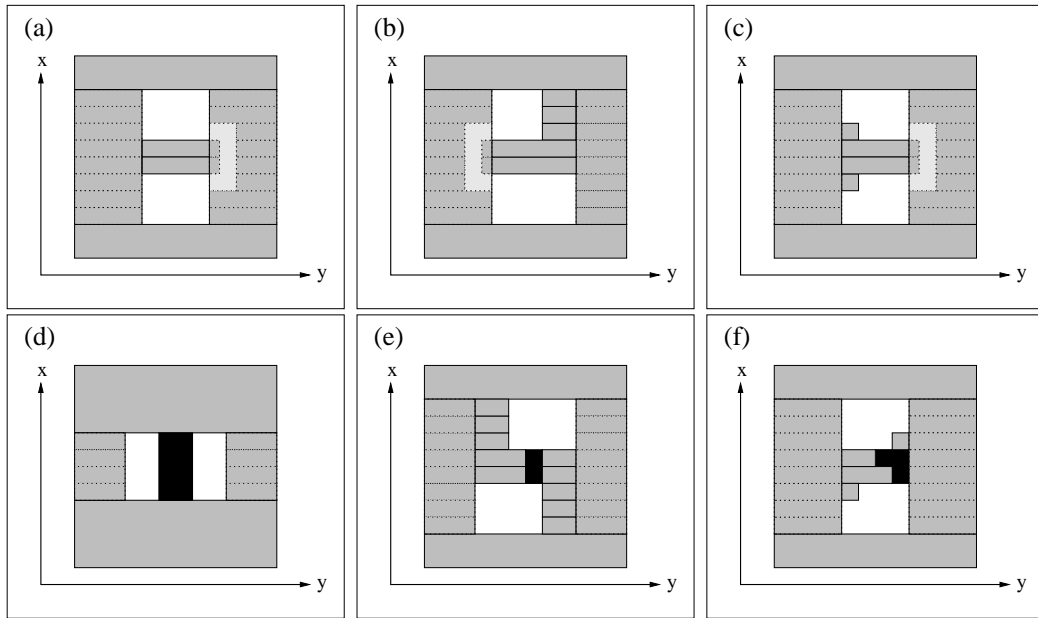


Figure 5.8: Examples for merging of segments. In three cases (a-c), merging of two segments results in a deliverable composite segment with valid leaf and diaphragm positions. In the other cases (d-f), merging introduces violations of the interdigitation constraint which can only be removed by adding additional areas (illustrated in black) to the composite segment. Therefore, merging of these pairs of segments is not performed.

5.1.7 Sorting of Segments

The final step of the segmentation sorts the remaining segments to achieve an efficient order for the delivery. The algorithm offers two ways of sorting the segments. Common to both, the largest segment is irradiated first. In this way, it is in most cases possible to record images of the whole treatment field for e.g. verification of the positioning of the patient before the treatment. Notice that the largest segment does not always comprise the whole field, because the latter may have been divided into two separate regions to block an OAR. After the first segment has been specified, the order of the other segments is determined step by step.

The first method minimizes the total leaf travel between subsequent segments. This parameter is calculated by summing the distance each leaf has to travel between two successive segments for all 80 leaves. The second segment is thus determined as the segment where this sum is minimal in combination with the first segment. The third

segment is chosen as the segment that has least total leaf travel in relation to the second and so on. This concept of sorting results in a fairly intuitive order of the segments. It is advantageous in terms of leaf positioning errors, because leaf movement is minimized. At present, this technique is used in clinical routine at the UKT.

The second concept minimizes the maximum leaf travel of any leaf between subsequent segments. The second segment is thus determined as the segment, where the maximum travel between the first and the second segment of any of the 80 leaves is minimal. This strategy is repeated for all the remaining segments. This method of sorting considers only the single leaf with the maximum travel distance between subsequent segments for the decision which segment to choose next. As a consequence, rather unintuitive series may result, where the total leaf travel is significantly increased compared to the first method. However, the second method is advantageous in terms of the time to deliver the series of segments, because the maximum distance that any leaf has to travel between subsequent segments determines the time interval between those segments.

Notice that both methods do not minimize the total leaf travel respectively the maximum leaf travel summed over the whole series of segments, but only pairwise between subsequent segments. Solutions for the minimization of the respective sums have to compare any combination of the whole series and are equivalent to a 'travelling-salesman'-problem. The presumably small improvements to be gained with such a strategy of sorting was not considered worth the increased time requirement for the computer calculation.

5.2 Reduction of the Number of Segments

In the previous sections, the conventional way of segmentation has been described. In this section, additional features of the algorithm are introduced, which are used to reduce the number of segments. Common to all these methods is the aim to eliminate either unimportant segments or segments with unsatisfactory properties. In contrast to the conventional segmentation, the new techniques allow modifications of the clustered profiles. However, these deviations can be compensated for if the sequencer is integrated into the dose optimization (see chapter 6).

5.2.1 Minimum Segment Weight Constraint

As already mentioned in section 4.2, the optimization of the fluence weight profiles considers the bandwidth of the clustering as a minimum fluence weight constraint. This restriction can be extended to a *minimum segment weight constraint*, which limits the minimum fluence weight of any segment. In this way, segments with fluence weights smaller than the bandwidth are eliminated after the conventional segmentation. This strategy reduces the number of segments and follows recommendations to restrict the number of segments

with very few monitor units [42].

5.2.2 Minimum Segment Size Constraint

Segments with a very small area can be eliminated by the specification of a *minimum segment size constraint*. If such a restriction is used, all segments with a size smaller than this constraint are eliminated as a final step of the segmentation prior to the sorting of the segments. If a minimum segment size constraint has not been defined, the size of any segment is determined by the product of leaf width and minimum gap constraint. However, it is generally desirable to avoid very small segments due to the difficult dosimetry of such fields [64] and the consequential decrease of treatment efficiency.

It is advisable to synchronize the minimum segment size constraint with the minimum segment width constraint because both constraints work in the same direction. A minimum segment size constraint of 4 cm^2 may e.g. be combined with a minimum segment width constraint of 2 cm.

5.2.3 Extended Merging

The conventional way of merging of segments considers only segments which have equal monitor units (see section 5.1.6). This method can be extended to also incorporate segments whose difference in monitor units is smaller than a given threshold. If such segments are successfully merged, the number of monitor units of the new segment is calculated as the area-weighted mean value of the monitor units of both segments. In analogy to the conventional merging, the segments to be merged are eliminated and the leaf positions of the composite segment are calculated.

5.2.4 Extended Superimposition

Sequencing with a small bandwidth results in a close approximation of the optimized profiles by the clustered profiles. However, profiles with numerous clusters may also lead to many very similar segments. To reduce the number of segments in these situations, the method for superimposition of segments as described in section 5.1.5 can be extended to eliminate not only segments with identical shape, but also ones with similar shape.

The process of extended superimposition starts with the determination of the degree of similarity between segments. Segments may differ in shape, which is measured by the number of different fluence weight elements, and fluence weight, which is determined by the difference in monitor units of both segments. In this way, the product of the number of different fluence weight elements and the difference in monitor units can be used to specify the difference respectively the similarity of segments. It can be measured in relation to the product of the minimum segment size constraint and the minimum segment weight

constraint. In the current clinical implementation of the sequencer at the UKT, pairs of segments are considered for extended superimposition if their difference is smaller than twice this product. Notice that these products are measures of the energy flux.

Any pair of such similar segments is superimposed to create a new segment with the smallest flux deviation from both segments. In this way, a kind of mean segment is created. Its fluence weight is determined by the sum of the monitor units of both segments. The area that both segments have in common is part of the new segment. For fluence weight elements which are part of only one of the segments, the initially optimized fluence weight value is compared to half of the weight of the new segment. If it is smaller, the fluence weight element is eliminated, otherwise it is added to the new segment. The initially optimized instead of the clustered fluence weight of any element is used in order to consider the optimized dose distribution as closely as possible for the extended superimposition. The new segment may be different in shape to both the old segments, as can be seen in an 1D example in figure 5.9.

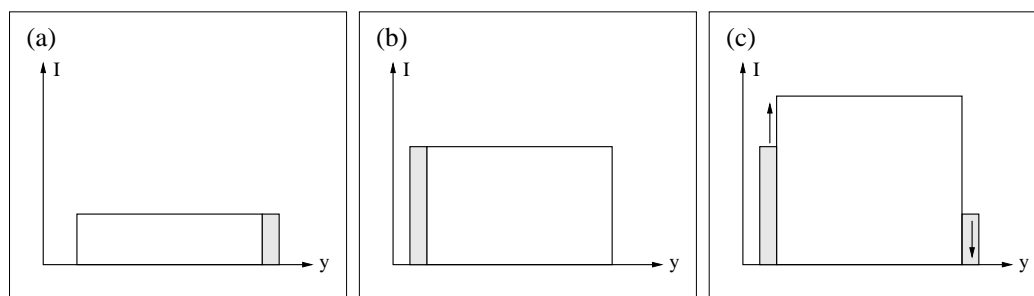


Figure 5.9: Example for the extended superimposition of two 1D segments. While the center part of both segments are equivalent, the first segment is slightly larger on the right side (a) and the second segment on the left side (b). The new segment is created by using the area that is common to both segments and those fluence weight elements which are equal to or greater than half of the new number of monitor units. As a consequence, the fluence weight element on the left is added to the new segment, while the right element is eliminated (c).

Notice that the resulting new segment may not be deliverable if it e.g. consists of two separate regions to be irradiated in direction of leaf motion. If this is the case, extended superimposition of segments is not performed. Otherwise, the two old segments are eliminated and the leaf positions of the new segment are calculated. Examples for a successful and an unsuccessful extended superimposition of segments are illustrated in figure 5.10.

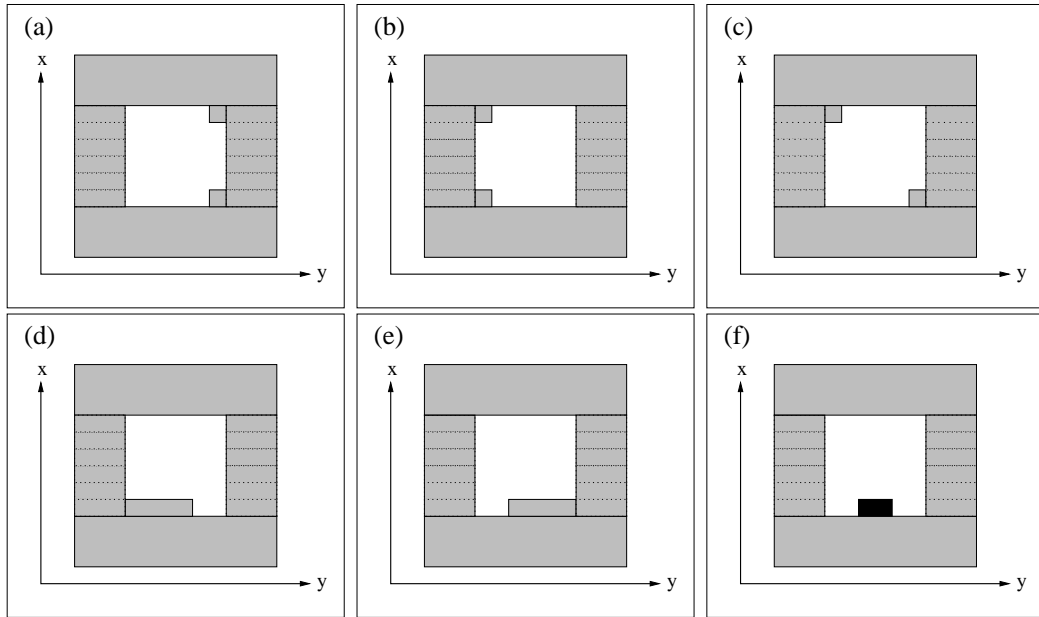


Figure 5.10: Examples for successful and unsuccessful extended superimposition of two 2D segments. The first pair of segments (a-b) can be combined to form a deliverable composite segment (c). In contrast to that, extended superimposition of the second pair (d-e) results in a segment which is not suitable, as it cannot block the area illustrated in black (f). Therefore, extended superimposition for the second pair is not performed.

5.3 Features of the Segmentation Algorithm

In the previous sections of this chapter, the segmentation algorithm has been presented in all its details. In this section, some of the general features of the algorithm are highlighted and discussed.

5.3.1 Sliding-Window vs. Close-In

Most of the published sequencers deliver the series of segments with the sliding-window-technique, where all leaves move uni-directionally (see section 3.2). Although this method is very time-efficient, it is not possible to deliver the whole treatment field as the first segment for setup verification. A previous publication proposed to use the sliding-window-technique for all but the first segment to eliminate this drawback [76]. However, the modified sliding-window-technique is less time-efficient.

Our sequencer neither uses the sliding-window-technique nor a strict close-in-technique. The segmentation aims at solutions with few and optimally-shaped segments. Furthermore, the largest segment is delivered first. In this way, the direction of leaf motion is not restricted at all between subsequent segments.

5.3.2 Tongue&Groove-Effect

Our sequencing method does not completely eliminate the tongue&groove-effect, but reduces the number of occurrences. In most cases, horizontal matchlines between segments are avoided by replacing them by vertical ones (see section 5.1.3). However, a horizontal split of a segment due to the interdigitation constraint as illustrated in figure 5.2 d may occur.

In principle, it is possible to completely avoid the tongue&groove-effect. An example for such a strategy is demonstrated in figure 5.11. Here, the horizontal cut can be replaced by a vertical one, if the y-diaphragms are used in combination with the opposing leaves to define a segment width smaller than the minimum gap constraint in direction of leaf motion. Although this concept may eliminate any appearance of the tongue&groove-effect, it has serious disadvantages. First of all, the exposure is increased in regions where only the y-diaphragms shield the irradiation. More importantly, the technique introduces field dimensions smaller than the minimum gap constraint and thus typically smaller 1 cm in direction of leaf motion. As mentioned in section 5.2.2, such fields are problematic from a dosimetric point of view. As a consequence, we did not incorporate this strategy to completely eliminate the tongue&groove-effect. Further details about the dosimetric consequences of the tongue&groove-effect are given in section 7.4.

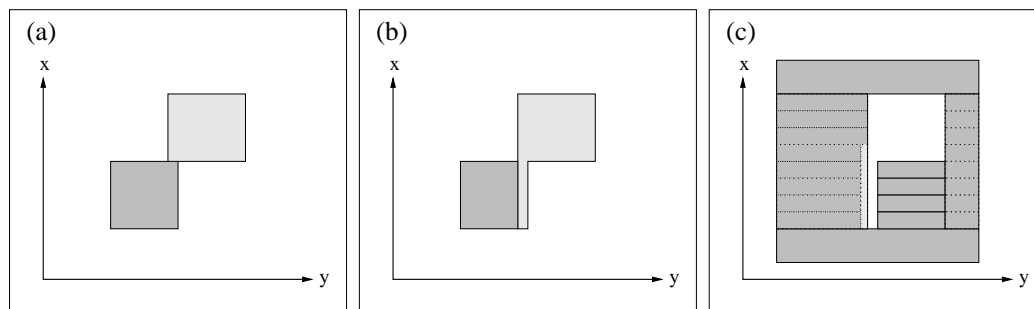


Figure 5.11: Example for a strategy to completely avoid the tongue&groove-effect. The horizontal split of the pre-segment due to the interdigitation constraint (a) can be replaced by a vertical cut (b). In this case, the second segment contains a small region (illustrated in (c) in light gray) that can only be shielded by the left y-diaphragm due to the minimum gap constraint between opposing leaves.

5.3.3 Approximation of the Clustered Profiles

The way of segmentation as described in section 5.1 does not modify the clustered profile, i.e. the resulting series of segments exactly reproduces the profile. This strategy prevents that the sequencer consists of a long chain of procedures that individually introduce modifications of the initially optimized profile.

However, the methods introduced in section 5.2 violate this principle and allow modifications of the profile during the segmentation to be able to e.g. reduce the number of segments. Such techniques have to be handled carefully, as otherwise unbalanced modifications of the dose distribution may result. For this reason, they can only be used reasonably if the sequencer is part of the optimization as introduced in the following chapter.

5.4 Performance of the Segmentation

In appendix A, the segmentation algorithm is applied as described in section 5.1 for the profiles used in section 4.4. In this section, the results are summarized. The mean values of the resulting number of segments are listed in table 5.1.

bandwidth [MU]	clusters	segments
38	2.9	3.7
19	4.2	5.5
9	7.9	11.7

Table 5.1: Results of the segmentation for three different values of the bandwidth averaged over the 10 profiles of appendix A. Listed are the number of clusters and the resulting number of segments.

A statistical measure of the segmentation is the segments to clusters ratio, which is about 1.3-1.5 for our test cases. The minimum value of this ratio is fixed by the complexity of the profile, in particular by the number of in-field minima in direction of leaf motion. For each profile, the minimum ratio was estimated through considerations about in-field minima, interdigitation violations and offsets from the center of the field. For all profiles, we achieved segments to clusters ratios close or equal to the minimum (for further details see appendix A). In this way, the segmentation resulted in a reasonably low number of segments.

Chapter 6

Integration into the Inverse Planning Algorithm

Conventional sMLC sequencers are applied in a final step before the delivery, after forward or inverse treatment planning. The introduced deterioration of the dose distribution is difficult to control, because sequencers usually consider fluence weights only. In general, sequencing with a low number of e.g. less than 5 fluence weight levels is expected to significantly deteriorate the dose distribution. In particular, violations of the prescribed dose restrictions may be introduced. An example of the resulting modifications is given in a cumulative *dose-volume-histogram* (DVH) in figure 6.1 for treatment planning of a head&neck case performed with HYPERION.

It is therefore indispensable to control and possibly compensate for the influence of the sequencing on the dose distribution. This can be achieved by either incorporating the sequencing into the optimization from the beginning, or by applying an additional step of re-optimization of the segments with respect to the dose distribution after the sequencing. While the first concept is a pure inverse approach, the second can also be combined with forward treatment planning. Actually, most of the published methods to re-optimize the segments use forward planning strategies to define the initial segments [28,30,36,85]. The re-optimization is performed with an objective function that reflects the desired dose distribution. Usually, it concerns only the weights of the segments. However, a recent publication extended the re-optimization to also consider segment shapes [29]. Furthermore, first attempts to integrate the sequencing into the fluence weight profile optimization have been published [47,63].

In this chapter, we present a concept to integrate the sequencer into the inverse planning algorithm and to re-optimize the weights and shapes of the segments with respect to the dose distribution. At first, section 6.1 summarizes important features of the inverse planning algorithm. Afterwards, we introduce the principles of our method of re-

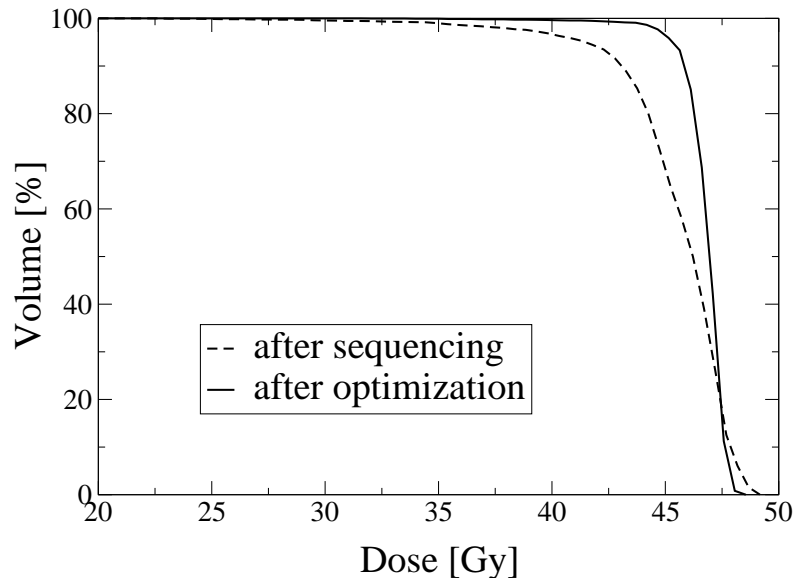


Figure 6.1: Cumulative DVH of the initially optimized dose distribution (solid line) and after the sequencing (dashed line) for one of the PTVs of a head and neck case optimized with HYPERION. While the optimized dose distribution meets the dose prescription, the sequencing results in a substantial deterioration.

optimization briefly, while further details can be found elsewhere [4]. Finally, we summarize the consequences for the use of our integrated sequencer.

6.1 Inverse Planning

During the last years, the inverse planning algorithm HYPERION has been developed at the UKT [1]. HYPERION optimizes fully modulated fluence weight profiles and maximizes the *equivalent uniform dose* (EUD¹) to the tumor under consideration of strict constraints for the OARs. In this way, HYPERION differs from most of the other inverse planning algorithms, which use weighting factors for tumors and OARs during the optimization [45].

Inverse planning is performed with an iterative optimization of a conjugate-gradient type. It minimizes an objective function, which reflects the dose prescriptions for tumor and OARs. The algorithm considers strict *constraints* for tumors and OARs and desired but not strict *objectives* for the tumor. In case of a conflict between an objective and a constraint, the latter has priority, so that e.g. the dose restrictions for an OAR are

¹The EUD is the homogeneous dose to a volume that results in the same dose response as the inhomogeneous, optimized dose distribution.

still satisfied, but the tumor dose is reduced in an overlap region between both structures. A variety of objectives and constraints can be specified, either considering physical properties like a quadratic overdose constraint, or biological models like the average tumor cell survival. A detailed description of the inverse planning algorithm can be found elsewhere [1–3, 5].

6.2 Re-Optimization of Segments

An inverse treatment planning procedure with *HYPERION* consists of three major steps. At first, the actual inverse planning is performed by optimizing fluence weight profiles from every beam direction as described in section 6.1. Afterwards, an initial sequencing transforms each fluence weight profile into a series of segments which are deliverable with the MLC (see chapters 4 and 5). Finally, the resulting segments are re-optimized with respect to the dose distribution. In this way, treatment planning with *HYPERION* is fully inverse. The user can choose between two ways of re-optimizing the segments. In the simpler approach, only the weights of the segments are considered in analogy to most of the other algorithms. However, it is also possible to perform a full re-optimization of the weights and the shapes of the segments. While the first method is very fast, the second is the method of choice to optimize a treatment plan in terms of the relation between the quality of the dose distribution and the number of segments.

The re-optimization is performed with almost the same objective function as the initial optimization of the fluence weight profiles. However, the weights and shapes of the segments are considered as additional parameters. A multistable penalty function is applied for all fluence weight elements at the borders of the segments. In this way, the shape of the segments may be altered if the new configuration results in a better dose distribution and if it is implementable with the MLC. In contrast to the series of segments after the initial sequencing, the re-optimization guarantees that the final series of segments strictly satisfies the specified restrictions for the OARs. A detailed description of the re-optimization can be found in [4]. Figure 6.2 illustrates a sketch of the inverse planning concept of *HYPERION*.

During the re-optimization, a modified segmentation of the new segment shapes is performed frequently to update the configuration of segments. In the following section, the specific implementation of the sequencer for the initial sequencing and for the re-optimization of segments is described briefly.

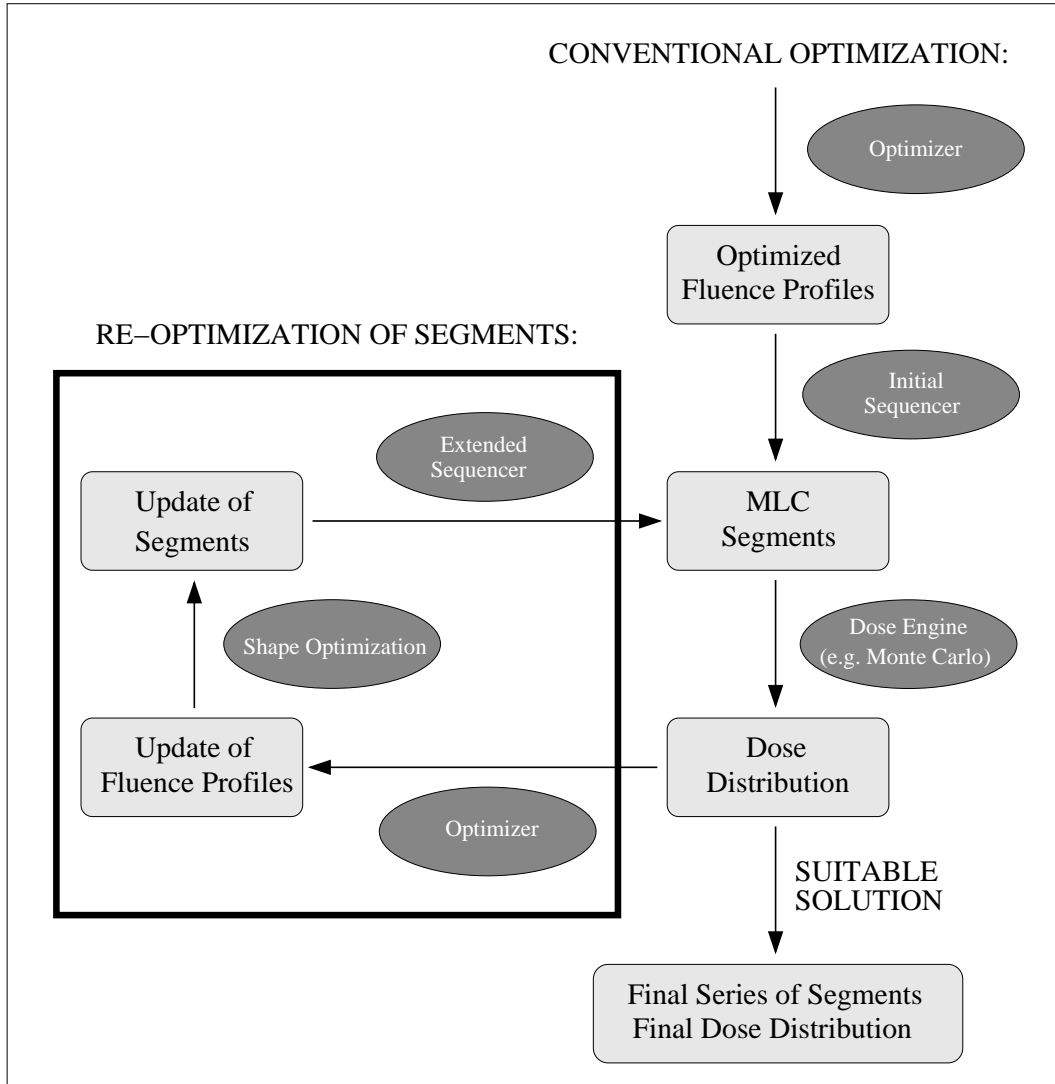


Figure 6.2: Illustration of the inverse planning concept of HYPERION. At first, an optimization of the fluence weight profiles takes place. Afterwards, the optimized profiles are transformed into implementable segments. The re-optimization of the segments is performed in a loop that includes dose calculation (e.g. with Monte Carlo), optimization of fluence weight profiles, optimization of the segment shapes and extended sequencing. The loop is finished, if the final series of segments results in a suitable dose distribution with respect to the dose prescription and the dose restrictions. Notice that conventional inverse planning strategies do not include a loop for the re-optimization of segments.

6.3 Integration of the Sequencing

After the optimization of the fluence weight profiles, the initial sequencing is performed to achieve a suitable initial set of segments as starting point. At first, each optimized profile is clustered and possible violations of the minimum gap and the maximum overtravel constraint are eliminated as described in chapter 4. Afterwards, the clustered profiles are segmented and conventional superimposition as well as merging of the segments is accomplished. Segments smaller than the minimum segment size constraint are eliminated. Finally, the resulting segments are sorted to minimize the total leaf travel between subsequent segments (see chapter 5).

During the re-optimization of segments, the sequencing is performed frequently. While clustering of the fluence weight profiles is not necessary any more, the algorithm eliminates possible violations of the minimum gap and the maximum overtravel constraint. Most of the parts of the segmentation are similar to those of the initial sequencing. However, as an additional step before the sorting of the segments, extended superimposition of the segments is performed.

Chapter 7

Performance of the Integrated Sequencer

In the previous chapters, the sequencer has been described in detail and results of clustering and segmentation have been presented. This chapter focuses on the performance characteristics of our inverse planning concept with integrated sequencer and its clinical application. In the following section, we analyze the correlation between the quality of the dose distribution and the number of segments to estimate the clinical efficiency of our method. Afterwards, we summarize the results of a treatment planning comparison of our inverse planning approach with a forward planning strategy for 10 head and neck cases. The background of this study is the question whether manual definition of the segment shapes in combination with an optimization of the segment weight is sufficient or if a full inverse approach for the determination of segment shapes and weights can further improve the quality of treatment plans. In section 7.3, we demonstrate the superiority of our inverse planning strategy with integrated sequencing compared to conventional inverse planning for a complex head and neck case. Furthermore, we discuss the tongue&groove-effect and finally describe the clinical implementation of our method at the UKT briefly.

7.1 Efficiency of Integrated Segment Optimization

Most inverse planning strategies separate the optimization of the dose distribution and the sequencing. As a consequence, the quality of the dose distribution and the number of segments as most important characteristics of the treatment plan are not or only weakly correlated. This may likely lead to insufficient dose distributions or, if no strategies to eliminate unimportant segments are applied, inefficient treatment plans due to a large number of segments and monitor units. We performed a treatment planning study with HYPERION and the integrated sequencer to test the hypothesis, that integration of the

sequencing into the optimization of the dose distribution has the potential to eliminate these problems (see also appendix B).

The correlation between the approximation of the clustering, the number of segments and the quality of the dose distribution was determined for inverse treatment planning of a nasopharynx case with 6 beam directions (see figure 7.1). The bandwidth of the clustering was varied between 1 and 8 MU. The EUD of the PTV, which is an intuitive measure of the objective function, was chosen to rank the quality of the dose distribution. As the dose restrictions for the OARs were always fulfilled due to the optimization concept of HYPERION, their variation for different values of the bandwidth was negligible. The results in terms of bandwidth, number of segments, and EUD are summarized in table 7.1.

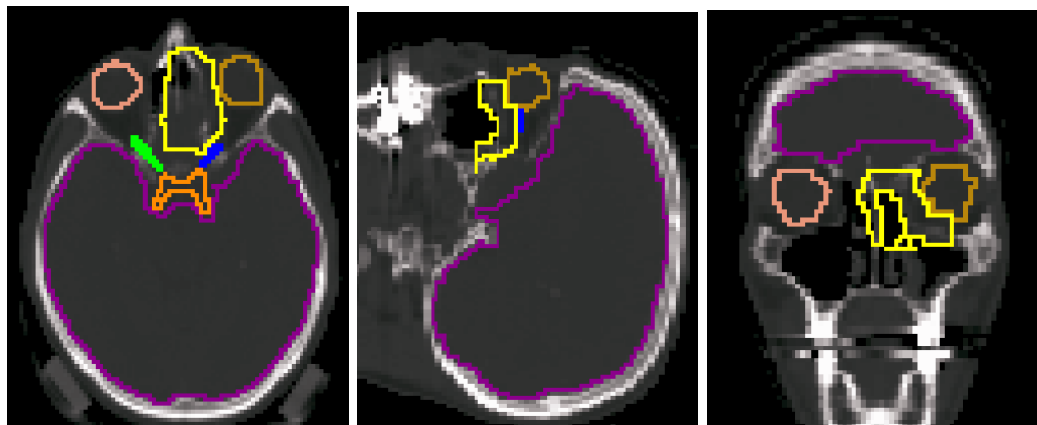


Figure 7.1: Illustration of the nasopharynx case in transversal, sagittal and coronal plane with the yellow contours of the tumour and those of the OARs in close proximity.

bandwidth [MU]	# segments	EUD [Gy]
1	46	70.1
2	41	70.1
3	27	69.8
4	29	69.9
5	20	69.3
6	22	69.5
7	17	68.7
8	15	67.8

Table 7.1: Results for the optimizations of the nasopharynx case in terms of number of segments and EUD for 8 values of the bandwidth.

In figure 7.2 a, the number of segments is plotted against the bandwidth. The larger the bandwidth, the coarser the approximation of the optimized profiles and the lower the number of segments. Notice that the curve is not strictly monotonous. This is due to local minima, which result from the discrete approximation of the quasi-continuous fluence weight profiles by the clustering algorithm. The quality of the treatment plan can be better visualized with a plot of the EUD of the PTV against the number of segments as shown in figure 7.2 b. The curve demonstrates the stable relation between the quality of the dose distribution and the number of segments. The larger the number of segments, the better the approximation of the optimized profiles and thus the quality of the dose distribution. Notice that the curve saturates at a certain number of segments, because additional segments do not further improve the dose distribution significantly.

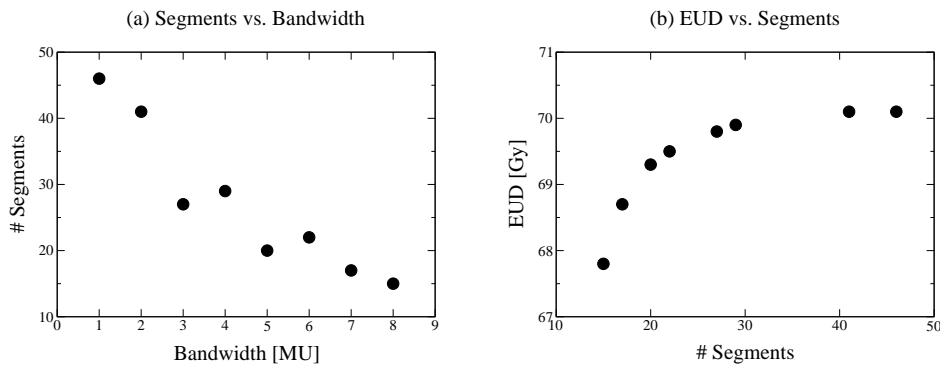


Figure 7.2: Results of the nasopharynx case are demonstrated with a plot of the number of segments versus the bandwidth (a) and the EUD of the PTV versus the number of segments (b).

In this complex nasopharynx case, a very conformal and efficient treatment plan with a high EUD and a low number of about 30 segments can be chosen for treatment. Similar results were achieved with a dose-escalated prostate case (see appendix B). These findings confirm the aforementioned hypothesis and demonstrate the high efficiency of our inverse planning concept with integrated sequencing.

7.2 Forward vs. Inverse Planning

A treatment planning comparison of forward and inverse planning was performed to study the impact of computer-optimized segment shapes and to estimate the benefits of the more complex inverse planning approach. Ten patients with head and neck cancer which had been treated with the forward planning approach described below at the Netherlands Cancer Institute (NKI) between October 2000 and January 2002 were selected for the comparison. A dose of 46 Gy was prescribed to the PTV for the main phase of the treatment and a

boost of typically 24 Gy to the areas of highest risk. The spinal cord and both parotid glands were considered as OARs. In particular, the aim of the treatment planning was to spare the parotid glands to avoid or suppress xerostomia without compromising the coverage of the PTV. We followed the recommendations of another publication to restrict the mean dose of left and right parotid gland to 26 Gy if possible [33].

Forward treatment planning of the main phase was performed with the 3D treatment planning system U-MPLAN of the University of Michigan [37], which is used in clinical routine at the NKI. 5-10 coplanar beam directions and 9-15 segments were defined manually. Afterwards, a segment weight optimization was performed with an objective function that reflected the aims of the treatment. If indicated, the resulting segment shapes and beam directions were further modified manually in a final step. The boost was planned similarly, although a segment weight optimization was not considered necessary for the 2-4 beam directions and 2-5 segments.

Inverse treatment planning of the main phase with HYPERION was performed with the same beam directions as for the forward planning. Likewise, the objective function reflected the aims of the treatment. The planning of the boost phase was performed with a similar objective function. In some cases, the same beam directions as for the forward planning were used, in others different incidences were specified, e.g. to reduce the dose to the parotid glands. Inverse planning resulted on average in about the threefold number of segments compared to forward planning.

The coverage of the PTV with inverse planning was sometimes similar, but most of the time significantly better than that of forward planning. In table 7.2, the summed mean doses of main phase and boost to left and right parotid glands are summarized for all 10 patients for both treatment planning approaches. In most of the patients, inverse planning reduced the dose to the parotid glands significantly. In three cases, inverse planning managed to spare a parotid gland that had been sacrificed during forward planning by reducing the mean dose to values below 26 Gy. In figure 7.3, the resulting mean doses of forward and inverse planning are illustrated in a histogram. For each patient, the resulting mean dose for the parotid gland with the clinically more important difference between both techniques is illustrated. The histogram clearly demonstrates the reduction of the mean dose with inverse planning.

The study demonstrates the potential of inverse planning and computer-optimization of segment shapes to improve dose distributions significantly at the cost of an increased number of segments. However, this increase is not serious, as treatments with less than 50 segments can be delivered in about the same time as conformal treatments [24].

Patient	Left PG [Gy]		Right PG [Gy]	
	FOR	INV	FOR	INV
1	44	26	23	19
2	29	23	52	53
3	65	64	24	21
4	21	21	20	21
5	37	23	25	20
6	26	19	24	22
7	39	26	18	18
8	16	13	17	12
9	25	21	24	20
10	26	21	35	39

Table 7.2: Results of forward (FOR) and inverse (INV) planning of both treatment phases with respect to the mean dose to the left and right parotid glands (PG) for all 10 patients.

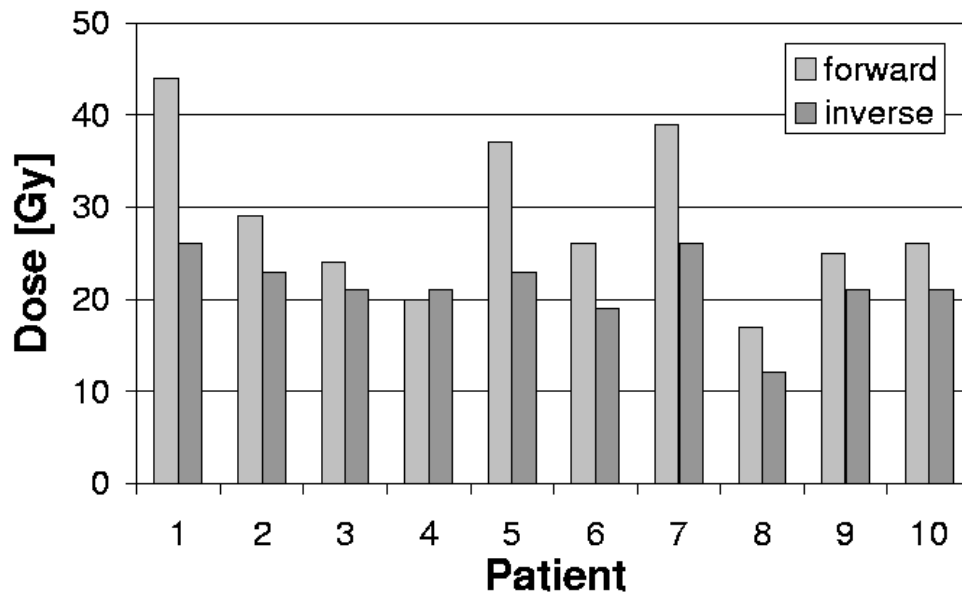


Figure 7.3: Histogram of the results for the mean dose to the parotid glands for all 10 patients after forward and inverse planning of both treatment phases. For each patient, the parotid gland with the clinically more important difference between both methods was chosen for this illustration (see table 7.2 for details).

7.3 Conventional vs. Integrated Sequencing

A treatment planning comparison between conventional inverse planning, i.e. sequencing is accomplished as a final step after the optimization of the fluence weight profiles, and our method, where sequencing is integrated into the optimization, was performed. The conventional strategy used HYPERION for optimization of the fluence weight profiles, the Bortfeld-Boyer method for clustering and our segmentation algorithm for the transformation of the clustered profiles into segments. The optimization-integrated concept used our sequencer and the integration scheme as described in chapter 6. As both strategies use HYPERION for the initial optimization of the fluence weight profiles, the resulting differences are determined by the different clustering algorithms and integration concepts of the sequencer. Our segmentation algorithm was used for both methods, because the published way of segmentation with the Bortfeld-Boyer method is not suitable for the Elekta MLC.

Treatment planning was performed for a complex head and neck patient, which had recently been used for a hitherto unpublished comparison of different inverse planning algorithms within the Elekta Consortium. Detailed information about this case can be found at <ftp://ri-exp.beaumont.edu/pub/msharpe/imrt/>. We chose this specific case for our comparison, because it is challenging with respect to appropriate treatment of the tumor and adequate number of segments. Less complex cases like e.g. prostate are usually not very demanding with regard to the number of segments.

Treatment planning and dose prescription followed the guidelines of the RTOG H-0022 protocol for a phase I/II study of conformal and intensity modulated irradiation of oropharyngeal cancer, which was developed by the Radiation Therapy Oncology Group (RTOG) of the American College of Radiology (ACR). Further information about this trial can be found at <http://rtog3dqa.wustl.edu>. Important dose prescriptions and limitations specific for our case are as follows: Treatment is scheduled for 30 fractions in 6 weeks with 5 daily fractions per week. The PTV consists of a primary PTV with a prescribed dose of 66 Gy (daily fraction of 2.2 Gy) and regions of subclinical disease with low (54 Gy, 1.8 Gy per day) and high (60 Gy, 2.0 Gy per day) risk. The maximum dose of the brain stem is restricted to 54 Gy and that of the spinal cord to 45 Gy. Another aim of treatment planning is to restrict the mean dose of each parotid gland to less than 26 Gy. In our case, the PTV consists of a single region with a prescription of 66 Gy, another with 54 Gy and two regions prescribed to 60 Gy. This geometry is illustrated in figure 7.4 in transversal, sagittal and coronal plane. Both inverse treatment planning approaches were performed with 7 coplanar, non-equidistant beams. Furthermore, the minimum segment weight was limited to 3 MU and the minimum segment size to 4 cm².



Figure 7.4: Illustration of the head and neck case in transversal, sagittal and coronal plane. The primary PTV with a prescription of 66 Gy is contoured in red, the region of subclinical disease with low risk (54 Gy) in green and the two regions of subclinical disease with high risk (60 Gy) in yellow and blue. The parotid glands are illustrated in orange and violet, brainstem and spinal cord in light and dark brown. Notice that the isocenter is marked with a white circle.

The results of the comparison were analyzed with respect to the dose distribution of the PTV and the number of segments. Dose limitations for the OARs are strictly satisfied due to the inverse planning concept of HYPERION. As a consequence, the results for OARs of both methods were similar and are not discussed in what follows. In figure 7.5, the cumulative DVHs of all four parts of the PTV are illustrated for our method with optimization-integrated sequencer (straight lines) and for the conventional strategy (dotted lines). The coverage of the primary PTV was in both cases satisfactory. Major differences between both strategies occurred for the other three parts of the PTV. Adequate coverage could only be achieved with the optimization-integrated method, while the conventional strategy resulted in serious underdosages. These results are illustrated in transversal, sagittal and coronal plane in figure 7.6 for the region of subclinical disease with low risk (contoured in green) and in figure 7.7 for one of the regions of subclinical disease with high risk (contoured in blue). The 54 Gy respectively 60 Gy isodose line is drawn in red in figures 7.6 and 7.7. These DVHs and dose distributions clearly demonstrate the superior results of our method with optimization-integrated sequencing and the insufficient coverage of the PTV by the conventional strategy. Furthermore, both methods differ explicitly with respect to the number of segments: While the conventional strategy resulted in a large number of 151 segments, the integrated method required only 79 segments.

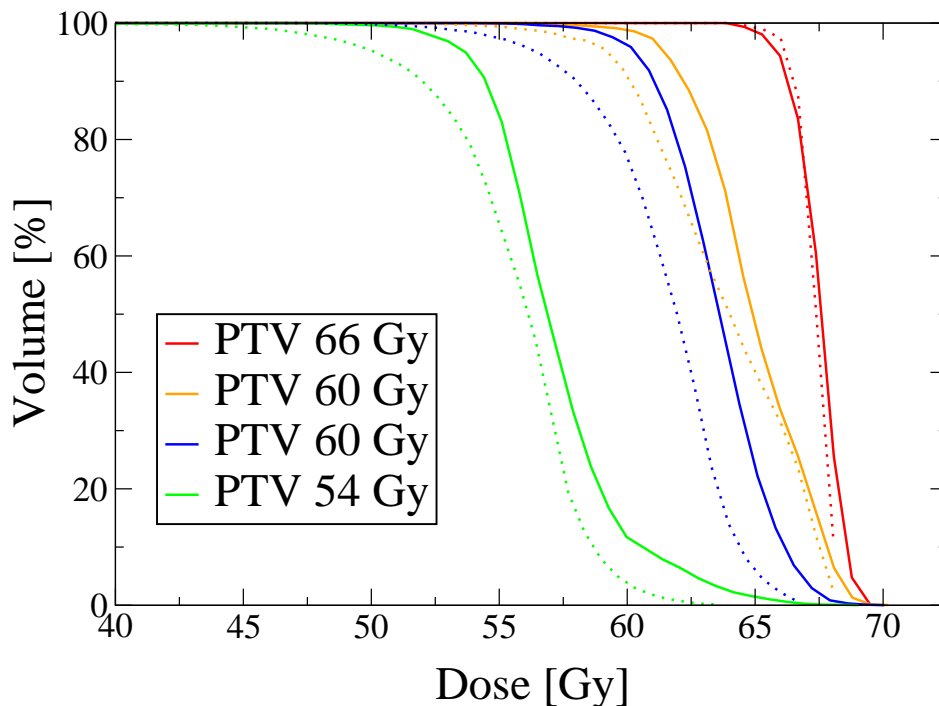


Figure 7.5: Cumulative DVHs of all four parts of the PTV for the integrated (straight lines) and the conventional strategy (dotted lines). The superior coverage of the regions of subclinical disease with low and high risk (illustrated in green, orange and blue) by the integrated method is clearly demonstrated. Notice that the yellow part of the PTV of figure 7.4 is illustrated in orange in this figure for better visibility.

In a second planning comparison, the procedure was slightly modified by using a minimum weight constraint of 3.5 MU instead of 3.0 MU and by slightly relaxing the dose limitations for the parotid glands to further reduce the number of segments. Inverse planning with the integrated method resulted in 45 segments and in 116 segments with the conventional strategy. The characteristics of the dose distributions are similar to that of the first comparison: Adequate coverage of all parts of the PTV for the integrated method and serious underdosage in three parts of the PTV for the conventional strategy.

These results demonstrate that our concept of optimization-integrated sequencing leads to explicitly better dose distributions in combination with a substantial reduction of the number of segments compared to a conventional inverse planning strategy. In general, optimization-integrated sequencing is superior to conventional inverse planning methods. In particular for complex cases like the presented head and neck case, it may be the only way to achieve clinically acceptable treatment plans.

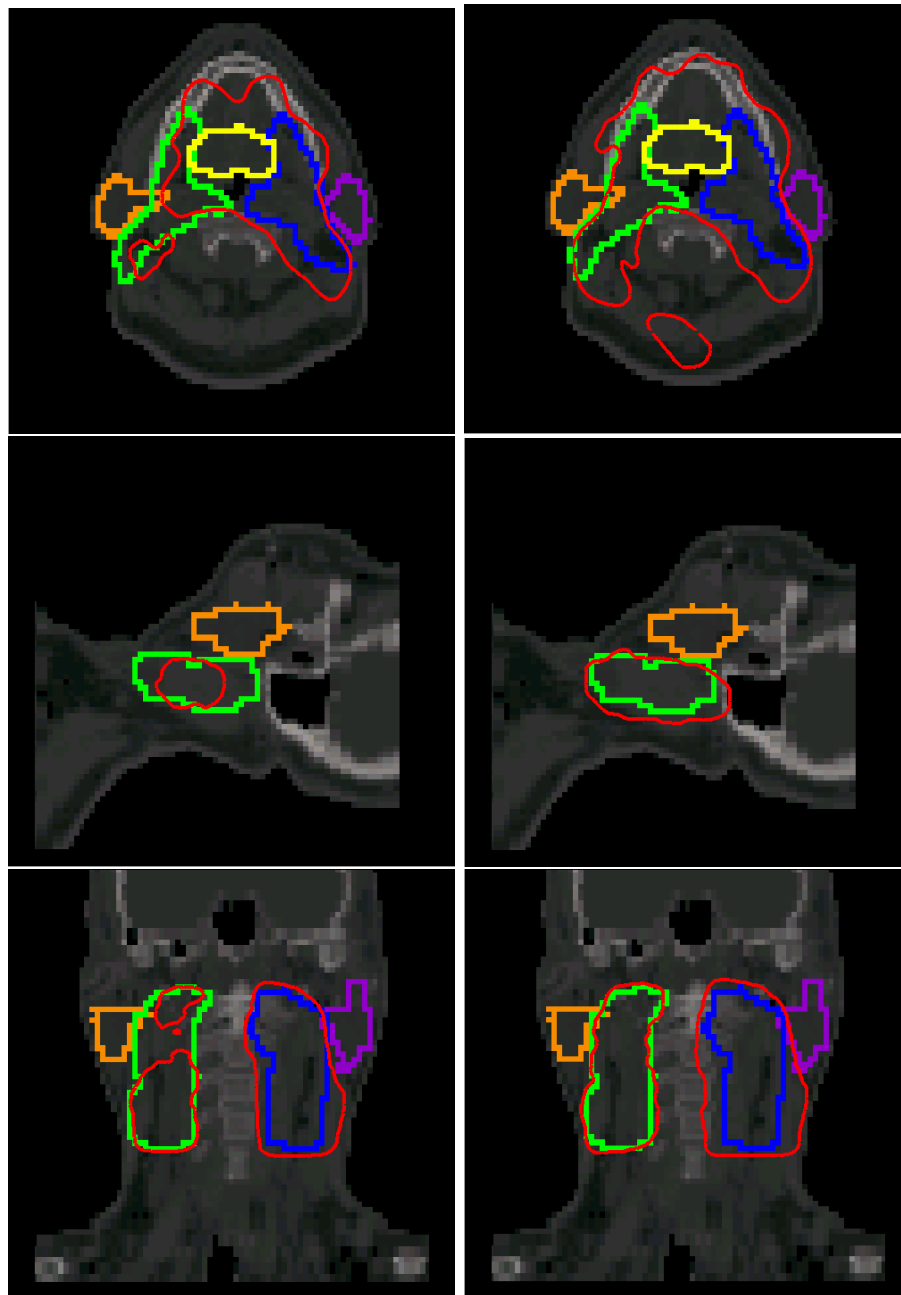


Figure 7.6: Dose distributions with respect to the region of subclinical disease with low risk (illustrated in green) in transversal, sagittal and coronal plane for the conventional method (left) and the integrated strategy (right). The red line illustrates the 54 Gy isodose line. While the integrated method adequately treats the green region, the conventional strategy leads to serious underdosage in parts of it.

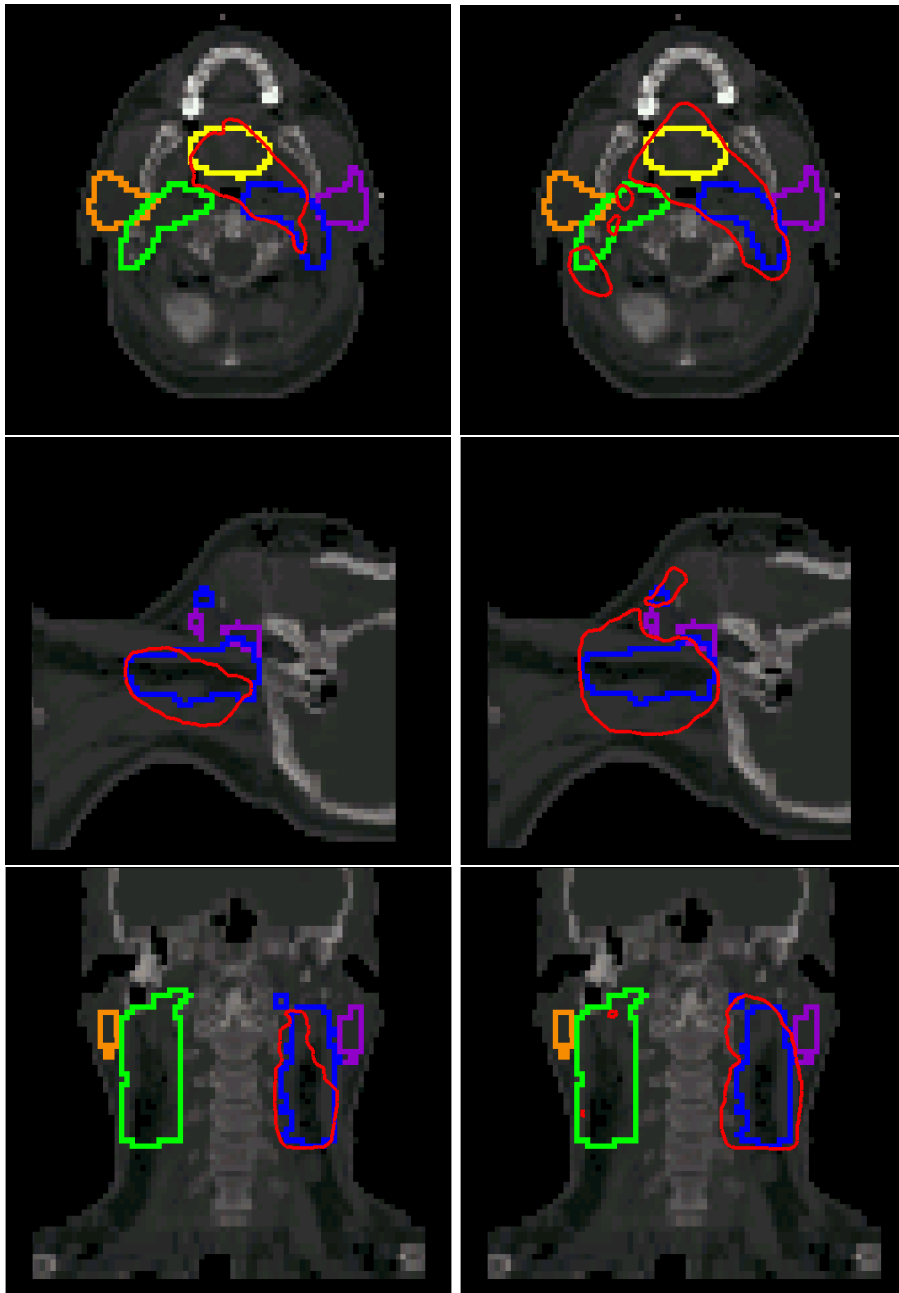


Figure 7.7: Dose distributions with respect to one of the regions of subclinical disease with high risk (illustrated in blue) in transversal, sagittal and coronal plane for the conventional method (left) and the integrated strategy (right). The red line illustrates the 60 Gy isodose line. While the integrated method adequately treats the blue region, the conventional strategy leads to serious underdosage in parts of it.

7.4 Tongue&Groove-Effect

As the tongue&groove-effect is usually not considered by the dose calculation, it is important to estimate its clinical impact. Sykes and Williams investigated the worst-case scenario of the effect for two adjacent segments shaped with an MLC and found a maximum underdosage of 15-28% and a full width at half maximum (FWHM) of about 4 mm [69]. At the UKT, measurements were performed for adjacent segments similar to those illustrated in figure 3.3 to estimate the tongue&groove- and the leaf-end-effect for our Elekta MLCs. Similar to the results of Sykes, the maximum underdosage due to the tongue&groove-design was found to be 25-30% with a FWHM of about 4 mm. Furthermore, the leaf-end-effect resulted in a maximum underdosage of about 15% and a FWHM of 4 mm. Another publication examined the tongue&groove-effect for clinical cases with Monte Carlo simulations by comparing dose distributions that neglect the effect and those that consider it [31]. They found no clinical significance of the effect for IMRT treatments with 5 or more beam directions due to the smearing effect of the individual fields.

These results confirm our concept to avoid the tongue&groove-effect if this is possible without major complications, but not at any cost. Furthermore, our solution of how to deal with the interdigitation constraint introduces matchlines, which will on average be short (see chapter 5).

7.5 Clinical Implementation

In Oktober 2001, inverse treatment planning with HYPERION was clinically introduced at the UKT to treat patients with prostate cancer. The clinical implementation uses HYPERION for inverse planning and the clinically validated treatment planning system PINNACLE for contouring, dose verification and communication with the linear accelerator [6]. Inverse planning is performed with a class solution of 5 equidistant, coplanar beam directions. For the 10 patients treated so far, on average 244 monitor units for a 2 Gy fraction and 21 segments were used (see table 7.3). In this way, on average 4.2 segments were delivered per beam direction. Neither treatment time nor workload for quality assurance procedures increased substantially. As a consequence, head and neck has been introduced as a second tumor site at our hospital and treatment of the first patient started in May 2002.

patient	1	2	3	4	5	6	7	8	9	10
segments	27	15	15	28	12	17	16	32	16	31
MU	251	225	235	320	217	229	219	265	221	262

Table 7.3: Summary of the total number of monitor units for a 2 Gy fraction and the number of segments for the first 10 IMRT treatments of patients with prostate cancer at the UKT.

Chapter 8

Conclusion

A major difficulty of treatment planning for sMLC are the limitations of the technical equipment, in particular those of the MLC. At present, most planning strategies neglect these restrictions during the optimization of the dose distribution. As a consequence, the optimized fluence weight profiles are not directly transformable into MLC-deliverable segments. Modifications of the profiles by the sequencing are necessary and lead to uncontrolled deterioration of the initially optimized dose distribution. Furthermore, the concepts of sequencing are often formulated in a rather general mathematical way and not directly adopted for a specific MLC. Many algorithms are thus not well suited to deal with complex limitations like the interdigitation constraint. As a consequence, unnecessarily many and insufficiently shaped segments may result. To deal with and eliminate these problems, a sequencing algorithm was developed, which is integrated into the optimization of the dose distribution and whose concept considers the specific limitations of the Elekta MLC.

The clustering algorithm projects the optimized fluence weight profiles onto piecewise constant profiles with few fluence weight steps of variable size. In this way, the clustered profiles approximate the ideal profiles closely. A comparison of the conventional method with equidistant fluence weight steps and our strategy for a given number of fluence weight steps demonstrated the superiority of our method for several mathematical and clinical test cases. Furthermore, our strategy takes the limitations of the MLC into account, so that the clustered profiles are directly transformable into deliverable segments and no further modifications during the segmentation are necessary.

The segmentation algorithm, which transforms the clustered profiles into a series of implementable segments, is specifically designed for the restrictions of the Elekta MLC. Several methods are applied to reduce the number of segments by eliminating unimportant segments and to result in a series of reasonable segments from a practical and dosimetric point of view. The user can thus define constraints for e.g. the minimum fluence weight, the minimum segments size or the minimum segment width. The algorithm prevents

underdosage due to the tongue&groove-effect most of the time, only in situations where the avoidance would have worse consequences, it is accepted. The order of the resulting series of segments is arranged to minimize the total leaf travel distance between subsequent segments. Furthermore, the treatment starts with the largest segment, so that it is possible to record verification images of the whole radiation field before the treatment. To be able to consider all aims and limitations of the delivery in an appropriate way, our concept of segmentation is neither performed in pure sliding-window- nor close-in-technique. The segmentation of several clustered test cases demonstrated the efficiency of our algorithm.

The sequencer was integrated into the optimization of the dose distribution of our inverse planning algorithm HYPERION. The inverse planning procedure starts with an optimization of the fluence weight profiles, followed by an initial sequencing, which results in a first guess of the series of segments. Afterwards, shape and fluence weight of the segments are considered in the objective function and re-optimized with respect to the dose distribution. In this way, modifications of the dose distribution due to the sequencing are well-controlled and the final series of segments strictly fulfills the dose prescription. The performance of our inverse planning concept with integrated sequencer was analyzed in three planning studies for several patients with head and neck tumors. The first study demonstrated the efficiency of our concept in terms of the correlation between the number of segments and the quality of the dose distribution. In the second study, the results of our method were compared to those of a forward planning strategy for sMLC delivery. In all cases, we achieved acceptable treatment plans with less than 50 segments divided among 5-10 beam directions. In most cases, our method improved the coverage of the PTV and/or the sparing of the parotid glands significantly in combination with an acceptable increase of the number of segments. The third study compared the results of our inverse planning concept with optimization-integrated sequencing to a conventional method of inverse planning for a complex head and neck case. While the conventional method failed to achieve adequate coverage of the PTV and a clinically acceptable number of segments, our strategy resulted in an appropriate treatment plan with respect to the dose distribution and the number of segments. These findings demonstrate the superiority and necessity of inverse planning with optimization-integrated sequencing.

In October 2001, our inverse planning approach was clinically introduced at the UKT to treat patients with prostate tumors. At present, 10 patients have been treated with on average 244 monitor units and 21 segments divided among 5 equidistant beam directions. Neither treatment time nor workload for quality assurance procedures increased substantially. As a consequence, head and neck has been introduced as a second tumor site at our hospital and a first sMLC treatment of a complex case started in May 2002.

Nowadays, there is general agreement that IMRT has the potential to improve the quality of radiotherapy treatments with respect to clinical outcome significantly. How-

ever, there is also widespread scepticism, if it is possible to deliver IMRT efficiently with respect to time and workload requirements. In this thesis, a new concept to deliver IMRT with sMLC was developed and integrated into an inverse planning algorithm. Its performance characteristics show very good dose distributions in combination with highly efficient delivery. These results give evidence that it is possible to introduce IMRT as the standard treatment technique for a large number of patients.

Bibliography

- [1] M. Alber, M. Birkner, W. Laub, and F. Nüsslin. Hyperion - an integrated IMRT planning tool. In *Proc. 13th Int. Conf. on the Use of Computers in Radiation Therapy*, pages 46–48. Heidelberg: Springer, 2000.
- [2] M. Alber and F. Nüsslin. An objective function for radiation treatment optimization based on local biological measures. *Phys. Med. Biol.*, 44:479–493, 1999.
- [3] M. Alber and F. Nüsslin. Intensity modulated photon beams subject to a minimal surface smoothing constraint. *Phys. Med. Biol.*, 45:N49–N52, 2000.
- [4] M. Alber and F. Nüsslin. Optimization of intensity modulated radiotherapy under constraints for static and dynamic MLC delivery. *Phys. Med. Biol.*, 46:3229–3239, 2001.
- [5] M. L. Alber. *A concept for the optimization of radiotherapy*. PhD thesis, Eberhard-Karls-Universität zu Tübingen, 2000.
- [6] W. Bär, M. Alber, M. Birkner, A. Bakai, A. Mondry, O. Dohm, G. Christ, and F. Nüsslin. Ein Konzept zur klinischen Implementierung von IMRT am Beispiel der Prostatabestrahlung. In *Jahrestagung der Deutschen Gesellschaft für Medizinische Physik*, pages 175–176. Neuried: ars una Verlagsdruckerei, 2001.
- [7] A. W. Beavis, P. S. Ganney, V. J. Whitton, and L. Xing. Optimization of the step-and-shoot leaf sequence for delivery of intensity modulated radiation therapy using a variable division scheme. *Phys. Med. Biol.*, 46:2457–2465, 2001.
- [8] R. Boesecke, J. Doll, B. Bauer, W. Schlegel, O. Pastyr, and W. J. Lorenz. Treatment planning for conformation therapy using a multileaf collimator. *Strahlenther. Onkol.*, 164:151–154, 1988.
- [9] T. Bortfeld, U. Oelfke, and S. Nill. What is the optimum leaf width of a multileaf collimator? *Med. Phys.*, 27:2494–2502, 2000.

-
- [10] T. R. Bortfeld, D. L. Kahler, T. J. Waldron, and A. L. Boyer. X-ray field compensation with multileaf collimators. *Int. J. Radiat. Oncol. Biol. Phys.*, 28:723–730, 1994.
- [11] A. L. Boyer, T. G. Ocran, C. E. Nyerick, and T. J. Waldron. Clinical dosimetry for implementation of a multileaf collimator. *Med. Phys.*, 19:1255–1261, 1992.
- [12] A. L. Boyer and C. X. Yu. Intensity-modulated radiation therapy with dynamic multileaf collimators. *Semin. Radiat. Oncol.*, 9:48–59, 1999.
- [13] A. Brahme. Design principles and clinical possibilities with a new generation of radiation therapy equipment. *Acta Oncologica*, 26:403–412, 1987.
- [14] A. Brahme. Optimization of stationary and moving beam radiation therapy techniques. *Radiother. Oncol.*, 12:129–140, 1988.
- [15] G. J. Budgell. Temporal resolution requirements for intensity modulated radiation therapy delivered by multileaf collimators. *Phys. Med. Biol.*, 44:1581–1596, 1999.
- [16] G. J. Budgell, C. Martens, and F. Claus. Improved delivery efficiency for step and shoot intensity modulated radiotherapy using a fast-tuning magnetron. *Phys. Med. Biol.*, 46:N253–N261, 2001.
- [17] G. J. Budgell, J. H. L. Mott, J. P. Logue, and A. R. Hounsell. Clinical implementation of dynamic multileaf collimation for compensated bladder treatments. *Radiother. Oncol.*, 59:31–38, 2001.
- [18] G. J. Budgell, J. R. Sykes, and J. M. Wilkinson. Rectangular edge synchronization for intensity modulated radiation therapy with dynamic multileaf collimation. *Phys. Med. Biol.*, 43:2769–2784, 1998.
- [19] C. Burman, C. S. Chui, G. Kutcher, S. Leibel, M. Zelefsky, T. LoSasso, S. Spirou, Q. Wu, J. Yang, J. Stein, R. Mohan, Z. Fuks, and C. C. Ling. Planning, delivery, and quality assurance of intensity-modulated radiotherapy using dynamic multileaf collimator: A strategy for large-scale implementation for the treatment of carcinoma of the prostate. *Int. J. Radiat. Oncol. Biol. Phys.*, 39:863–873, 1997.
- [20] E. B. Butler, B. S. Teh, W. H. Grant, B. M. Uhl, R. B. Kuppersmith, J. K. Chiu, D. T. Donovan, and S. Y. Woo. SMART (simultaneous modulated accelerated radiation therapy) boost: A new accelerated fractionation schedule for the treatment of head and neck cancer with intensity modulated radiotherapy. *Int. J. Radiat. Oncol. Biol. Phys.*, 45:21–32, 1999.
- [21] M. Carol, W. H. Grant, A. R. Blier, A. A. Kania, H. S. Targovnik, E. B. Butler, and S. W. Woo. The field-matching problem as it applies to the Peacock three

- dimensional conformal system for intensity modulation. *Int. J. Radiat. Oncol. Biol. Phys.*, 34:183–187, 1996.
- [22] M. P. Carol. Integrated 3-D conformal multivane intensity modulation delivery system for radiotherapy. In *Proc. 11th Int. Conf. on the Use of Computers in Radiation Therapy*, pages 172–173. Stockport, UK: Handley Printers Limited, 1994.
- [23] P. S. Cho and R. J. Marks. Hardware-sensitive optimization for intensity modulated radiotherapy. *Phys. Med. Biol.*, 45:429–440, 2000.
- [24] C. S. Chui, M. F. Chan, E. Yorke, S. Spirou, and C. C. Ling. Delivery of intensity-modulated radiation therapy with a conventional multileaf collimator: Comparison of dynamic and segmental methods. *Med. Phys.*, 28:2441–2449, 2001.
- [25] C. S. Chui, S. Spirou, and T. LoSasso. Testing of dynamic multileaf collimation. *Med. Phys.*, 23:635–641, 1996.
- [26] D. J. Convery and S. Webb. Generation of discrete beam-intensity modulation by dynamic multileaf collimation under minimum leaf separation constraints. *Phys. Med. Biol.*, 43:2521–2538, 1998.
- [27] J. Dai and Y. Zhu. Minimizing the number of segments in a delivery sequence for intensity-modulated radiation therapy with a multileaf collimator. *Med. Phys.*, 28:2113–2120, 2001.
- [28] E. M. F. Damen, M. J. P. Brugmans, A. van der Horst, L. Bos, J. V. Lebesque, B. J. Mijnheer, D. L. McShan, B. A. Fraass, and M. L. Kessler. Planning, computer optimization, and dosimetric verification of a segmented irradiation technique for prostate cancer. *Int. J. Radiat. Oncol. Biol. Phys.*, 49:1183–1195, 2001.
- [29] W. De Gersem, F. Claus, C. De Wagter, B. Van Duyse, and W. De Neve. Leaf position optimization for step-and-shoot IMRT. *Int. J. Radiat. Oncol. Biol. Phys.*, 51:1371–1388, 2001.
- [30] W. De Neve, W. De Gersem, S. Derycke, G. De Meerleer, M. Moerman, M. T. Bate, B. Van Duyse, L. Vakaet, Y. De Deene, B. Mersseman, and C. De Waeter. Clinical delivery of intensity modulated conformal radiotherapy for relapsed or second-primary head and neck cancer using a multileaf collimator with dynamic control. *Radiother. Oncol.*, 50:301–314, 1999.
- [31] J. Deng, T. Pawlicki, Y. Chen, J. Li, and S. B. Jiang C. M. Ma. The MLC tongue-and-groove effect on IMRT dose distributions. *Phys. Med. Biol.*, 46:1039–1060, 2001.

- [32] M. L. P. Dirkx, B. J. M. Heijmen, and J. P. C. van Santvoort. Leaf trajectory calculation for dynamic multileaf collimation to realize optimized fluence profiles. *Phys. Med. Biol.*, 43:1171–1184, 1998.
- [33] A. Eisbruch, R. K. Ten Haken, H. M. Kim, L. H. Marsh, and J. A. Ship. Dose, volume, and function relationships in parotid salivary glands following conformal and intensity-modulated irradiation of head and neck cancer. *Int. J. Radiat. Oncol. Biol. Phys.*, 45:577–587, 1999.
- [34] Elekta Precise Treatment System. *MLC Corrective Maintenance Manual Version 0C*, 1999.
- [35] P. M. Evans, V. N. Hansen, and W. Swindell. The optimum intensities for multiple static multileaf collimator field compensation. *Med. Phys.*, 24:1147–1156, 1997.
- [36] B. A. Fraass, M. L. Kessler, D. L. McShan, L. H. Marsh, B. A. Watson, W. J. Dusseau, A. Eisbruch, H. M. Sandler, and A. S. Lichter. Optimization and clinical use of multisegment intensity-modulated radiation therapy for high-dose conformal therapy. *Semin. Radiat. Oncol.*, 9:60–77, 1999.
- [37] B. A. Fraass and D. L. McShan. 3-D treatment planning: I. Overview of a clinical planning system. In *Proc. 9th Int. Conf. on the Use of Computers in Radiation Therapy*, pages 273–276. Amsterdam: North-Holland, 1987.
- [38] A. Frazier, M. Du, J. Wong, F. Vicini, R. Taylor, C. Yu, R. Matter, A. Martinez, and D. Yan. Dosimetric evaluation of the conformation of the multileaf collimator to irregularly shaped fields. *Int. J. Radiat. Oncol. Biol. Phys.*, 33:1229–1238, 1995.
- [39] J. M. Galvin, X. G. Chen, and R. M. Smith. Combining multileaf fields to modulate fluence distributions. *Int. J. Radiat. Oncol. Biol. Phys.*, 27:697–705, 1993.
- [40] P. B. Greer and T. van Doorn. A design for a dual assembly multileaf collimator. *Med. Phys.*, 27:2242–2255, 2000.
- [41] A. Gustafsson, B. K. Lind, R. Svensson, and A. Brahme. Simultaneous optimization of dynamic multileaf collimation and scanning patterns or compensation filters using a generalized pencil beam algorithm. *Med. Phys.*, 22:1141–1156, 1995.
- [42] V. N. Hansen, P. M. Evans, G. J. Budgell, J. H. L. Mott, P. C. Williams, M. J. P. Brugmans, F. W. Wittkämper, B. J. Mijnheer, and K. Brown. Quality assurance of the dose delivered by small radiation segments. *Phys. Med. Biol.*, 43:2665–2675, 1998.

- [43] A. R. Hounsell and T. J. Jordan. Quality control aspects of the Philips multileaf collimator. *Radiother. Oncol.*, 45:225–233, 1997.
- [44] M. S. Huq, Y. Yu, Z. P. Chen, and N. Suntharalingam. Dosimetric characteristics of a commercial multileaf collimator. *Med. Phys.*, 22:241–247, 1995.
- [45] Intensity Modulated Radiation Therapy Collaborative Working Group. Intensity-modulated radiotherapy: current status and issues of interest. *Int. J. Radiat. Oncol. Biol. Phys.*, 51:880–914, 2001.
- [46] T. J. Jordan and P. C. Williams. The design and performance characteristics of a multileaf collimator. *Phys. Med. Biol.*, 39:231–251, 1994.
- [47] M. A. Keller-Reichenbecher, T. Bortfeld, S. Levegrün, J. Stein, K. Preiser, and W. Schlegel. Intensity modulation with the "step and shoot" technique using a commercial MLC: A planning study. *Int. J. Radiat. Oncol. Biol. Phys.*, 45:1315–1324, 1999.
- [48] H. G. Kuterdem and P. S. Cho. Leaf sequencing with secondary beam blocking under leaf positioning constraints for continuously modulated radiotherapy beams. *Med. Phys.*, 28:894–902, 2001.
- [49] M. Langer, V. Thai, and L. Papiez. Improved leaf sequencing reduces segments or monitor units needed to deliver IMRT using multileaf collimators. *Med. Phys.*, 28:2450–2458, 2001.
- [50] N. Lee, P. Xia, J. M. Quivey, K. Sultanem, I. Poon, C. Akazawa, P. Akazawa, V. Weinberg, and K. K. Fu. Intensity-modulated radiotherapy in the treatment of nasopharyngeal carcinoma: An update of the UCSF experience. *Int. J. Radiat. Oncol. Biol. Phys.*, 53:12–22, 2002.
- [51] S. C. Lillicrap, H. M. Morgan, and J. T. Shakeshaft. X-ray leakage during radiotherapy. *Br. J. Radiol.*, 73:793–794, 2000.
- [52] C. C. Ling, C. Burman, C. S. Chui, G. J. Kutcher, S. A. Leibel, T. LoSasso, R. Mohan, T. Bortfeld, L. Reinstein, S. Spirou, X. H. Wang, Q. Wu, M. Zelefsky, and Z. Fuks. Conformal radiation treatment of prostate cancer using inversely-planned intensity-modulated photon beams produced with dynamic multileaf collimation. *Int. J. Radiat. Oncol. Biol. Phys.*, 35:721–730, 1996.
- [53] L. Ma, A. L. Boyer, L. Xing, and C. M. Ma. An optimized leaf-setting algorithm for beam intensity modulation using dynamic multileaf collimators. *Phys. Med. Biol.*, 43:1629–1643, 1998.

- [54] L. Ma, C. Yu, and M. Sarfaraz. A dosimetric leaf-setting strategy for shaping radiation fields using a multileaf collimator. *Med. Phys.*, 27:972–977, 2000.
- [55] T. R. Mackie, J. Balog, K. Ruchala, D. Shepard, S. Aldridge, E. Fitchard, P. Reckwerdt, G. Olivera, T. McNutt, and M. Mehta. Tomotherapy. *Semin. Radiat. Oncol.*, 9:108–117, 1999.
- [56] T. R. Mackie, T. Holmes, S. Swerdloff, P. Reckwerdt, J. O. Deasy, J. Yang, B. Paliwal, and T. Kinsella. Tomotherapy: A new concept for the delivery of dynamic conformal radiotherapy. *Med. Phys.*, 20:1709–1719, 1993.
- [57] S. L. Meeks, F. J. Bova, S. Kim, W. A. Tomé, J. M. Buatti, and W. A. Friedman. Dosimetric characteristics of a double-focused miniature multileaf collimator. *Med. Phys.*, 26:729–733, 1999.
- [58] C. Nutting, D. P. Dearnley, and S. Webb. Intensity modulated radiation therapy: a clinical review. *Br. J. Radiol.*, 73:459–469, 2000.
- [59] J. R. Palta, D. K. Yeung, and V. Frouhar. Dosimetric considerations for a multileaf collimator system. *Med. Phys.*, 23:1219–1224, 1996.
- [60] O. Pastyr, G. Echner, G. Hartmann, J. Richter, and W. Schlegel. Dynamic edge focussing: A new MLC-design to deliver IMRT with a double focussing high precision Multi-Leaf-Collimator. *Radiother. Oncol.*, 61:S24, 2001.
- [61] W. Que. Comparison of algorithms for multileaf collimator field segmentation. *Med. Phys.*, 26:2390–2396, 1999.
- [62] W. Schlegel, O. Pastyr, R. Kubesch, J. Stein, T. Diemer, K. H. Höver, and B. Rhein. A computer controlled micro-multileaf-collimator for stereotactic conformal radiotherapy. In *Proc. 12th Int. Conf. on the Use of Computers in Radiation Therapy*, pages 79–82. Madison, WI: Medical Physics Publishing, 1997.
- [63] J. Seco, P. M. Evans, and S. Webb. An optimization algorithm that incorporates IMRT delivery constraints. *Phys. Med. Biol.*, 47:899–915, 2002.
- [64] M. B. Sharpe, B. M. Miller, D. Yan, and J. W. Wong. Monitor unit settings for intensity modulated beams delivered using a step-and-shoot approach. *Med. Phys.*, 27:2719–2725, 2000.
- [65] R. A. C. Siochi. Minimizing static intensity modulation delivery time using an intensity solid paradigm. *Int. J. Radiat. Oncol. Biol. Phys.*, 43:671–680, 1999.

-
- [66] S. V. Spirou and C. S. Chui. Generation of arbitrary intensity profiles by dynamic jaws or multileaf collimators. *Med. Phys.*, 21:1031–1041, 1994.
- [67] J. Stein, T. Bortfeld, B. Dörschel, and W. Schlegel. Dynamic X-ray compensation for conformal radiotherapy by means of multi-leaf collimation. *Radiother. Oncol.*, 32:163–173, 1994.
- [68] R. Svensson, P. Källman, and A. Brahme. An analytical solution for the dynamic control of multileaf collimators. *Phys. Med. Biol.*, 39:37–61, 1994.
- [69] J. R. Sykes and P. C. Williams. An experimental investigation of the tongue and groove effect for the Philips multileaf collimator. *Phys. Med. Biol.*, 43:3157–3165, 1998.
- [70] J. S. Tsai, D. E. Wazer, M. N. Ling, J. K. Wu, M. Fagundes, T. DiPetrillo, B. Kramer, M. Koistinen, and M. J. Engler. Dosimetric verification of the dynamic intensity-modulated radiation therapy of 92 patients. *Int. J. Radiat. Oncol. Biol. Phys.*, 40:1213–1230, 1998.
- [71] S. van Dalen, M. Keijzer, H. Huizenga, and P. R. M. Storchi. Optimization of multileaf collimator settings for radiotherapy treatment planning. *Phys. Med. Biol.*, 45:3615–3625, 2000.
- [72] J. P. C. van Santvoort and B. J. M. Heijmen. Dynamic multileaf collimation without 'tongue-and-groove' underdosage effects. *Phys. Med. Biol.*, 41:2091–2105, 1996.
- [73] D. Verellen, N. Linthout, D. van den Berge, A. Bel, and G. Storme. Initial experience with intensity-modulated conformal radiation therapy for treatment of the head and neck region. *Int. J. Radiat. Oncol. Biol. Phys.*, 39:99–114, 1997.
- [74] S. Webb. *The Physics of Three-Dimensional Radiation Therapy: Conformal Radiotherapy, Radiosurgery and Treatment Planning*. Institute of Physics Publishing, 1993.
- [75] S. Webb. *The Physics of Conformal Radiotherapy: Advances in Technology*. Institute of Physics Publishing, 1997.
- [76] S. Webb. Configuration options for intensity-modulated radiation therapy using multiple static fields shaped by a multileaf collimator. *Phys. Med. Biol.*, 43:241–260, 1998.
- [77] S. Webb. A new concept of multileaf collimator (the shuttling MLC) - an interpreter for high-efficiency IMRT. *Phys. Med. Biol.*, 45:3343–3358, 2000.

- [78] S. Webb. *Intensity-Modulated Radiation Therapy*. Institute of Physics Publishing, 2001.
- [79] S. Webb, T. Bortfeld, J. Stein, and D. Convery. The effect of stair-step leaf transmission on the 'tongue-and-groove problem' in dynamic radiotherapy with a multileaf collimator. *Phys. Med. Biol.*, 42:595–602, 1997.
- [80] P. C. Williams and P. Cooper. High-resolution field shaping utilizing a masked multileaf collimator. *Phys. Med. Biol.*, 45:2313–2329, 2000.
- [81] Y. Wu, D. Yan, M. B. Sharpe, B. Miller, and J. W. Wong. Implementing multiple static field delivery for intensity modulated beams. *Med. Phys.*, 28:2188–2197, 2001.
- [82] P. Xia, P. Geis, L. Xing, C. Ma, D. Findley, K. Forster, and A. Boyer. Physical characteristics of a miniature multileaf collimator. *Med. Phys.*, 26:65–70, 1999.
- [83] P. Xia and L. J. Verhey. Multileaf collimator leaf sequencing algorithm for intensity modulated beams with multiple static segments. *Med. Phys.*, 25:1424–1434, 1998.
- [84] P. Xia and L. J. Verhey. Delivery systems of intensity-modulated radiotherapy using conventional multileaf collimators. *Med. Dosim.*, 26:169–177, 2001.
- [85] Y. Xiao, J. Galvin, M. Hossain, and R. Valicenti. An optimized forward-planning technique for intensity modulated radiation therapy. *Med. Phys.*, 27:2093–2099, 2000.
- [86] C. Yu, D. J. Chen, A. Li, L. Ma, D. Shapard, and M. Sarfaraz. Intensity-modulated arc therapy: clinical implementation and experience. In *Proc. 13th Int. Conf. on the Use of Computers in Radiation Therapy*, pages 164–166. Heidelberg: Springer, 2000.
- [87] C. X. Yu. Intensity-modulated arc therapy with dynamic multileaf collimation: an alternative to tomotherapy. *Phys. Med. Biol.*, 40:1435–1449, 1995.
- [88] C. X. Yu, M. J. Simons, M. N. Du, A. A. Martinez, and J. W. Wong. A method for implementing dynamic photon beam intensity modulation using independent jaws and a multileaf collimator. *Phys. Med. Biol.*, 40:769–787, 1995.
- [89] C. X. Yu, D. Yan, M. N. Du, S. Zhou, and L. J. Verhey. Optimization of leaf positions when shaping a radiation field with a multileaf collimator. *Phys. Med. Biol.*, 40:305–308, 1995.
- [90] M. J. Zelefsky, Z. Fuks, L. Happersett, H. J. Lee, C. C. Ling, C. M. Burman, M. Hunt, T. Wolfe, E. S. Venkatraman, A. Jackson, M. Skwarchuk, and S. A. Leibel. Clinical experience with intensity modulated radiation therapy (IMRT) in prostate cancer. *Radiother. Oncol.*, 55:241–249, 2000.

- [91] Y. Zhu, A. L. Boyer, and G. E. Desobry. Dose distributions of x-ray fields as shaped with multileaf collimators. *Phys. Med. Biol.*, 37:163–173, 1992.

Appendix A

A variable fluence step clustering and segmentation algorithm for step and shoot IMRT

published in Physics in Medicine and Biology **46** p.1997-2007 (2001).

Appendix B

Fluenzmodulierte Strahlentherapie mit in die Optimierung integrierter Segmentierung

accepted for publication in Zeitschrift für Medizinische Physik.

Acknowledgments

This thesis would have been impossible to realize without the help of numerous persons. I would like to thank in particular

Prof. Dr. Fridtjof Nüsslin who supported me in any imaginable way. He gave my scientific work direction and focus as well as productive freedom to spend 4 months in Amsterdam and to participate in several scientific meetings.

Dr. Markus Alber for guiding me scientifically through these three years by always showing me the right directions and giving me competent advice in any situation.

Annemarie Bakai, Mattias Birkner and Gustav Meedt for sharing happiness and sorrow of being a Ph.D. student as well as numerous beers and caipirinas on Thursday night at Tangente. I enjoyed drinking strange tea and fruit juices of the strawberry-spinach-type with Anne, playing badminton and finally even soccer with Mattias and proving that my taste of music is better than Gustav's...

Dr. Matthias Fippel, Freddy Haryanto and Oliver Dohm, our Monte Carlo group, for showing me that there are really other interesting research topics beside HYPERION. I still wonder if Freddy is a spy and if he stole my algorithm and sold it to the CIA...

Daniela Buck und Christoph Baum, our young group members, as well as the rest of the department of Medical Physics at the UKT for making our working climate a pleasant one.

Marco Schwarz, Dr. Luc Bos, Dr. Christoph Schneider, Dr. Ben Mijnheer, Dr. John Cho, Dr. Eugene Damen and the rest of the staff at the NKI in Amsterdam, who made my four months there a great time from a scientific as well as a personal point of view.

Christine for life beside physics.

Lebenslauf

- Geburt am 14.10.1972 in Erlangen als Sohn von Helga und Wolfgang Bär.
- Schulausbildung von 1979 bis 1992 in Erlangen, abgeschlossen mit dem Abitur.
- Von August 1992 bis Oktober 1993 Zivildienst bei den Regnitzwerkstätten für Behinderte in Erlangen.
- Studium der Physik mit Abschluß Diplom von November 1993 bis August 1999, bis zum Vordiplom an der Universität Bayreuth und anschließend an der Universität zu Köln. Zwischen Juni 1998 und August 1999 Anfertigung der Diplomarbeit *Fraktale Leitwertfluktuationen an metallischen Nanostrukturen* am Institut für Angewandte Physik der Universität zu Köln in der Arbeitsgruppe von Prof. Dr. R. Groß.
- Seit Oktober 1999 Anfertigung der Disseration mit dem Titel *Optimized delivery of intensity-modulated radiotherapy* in der Abteilung für Medizinische Physik der Eberhard-Karls-Universität Tübingen unter Anleitung von Prof. Dr. F. Nüsslin.
- Von Oktober 2001 bis Januar 2002 Forschungsaufenthalt am Nederlands Kanker Instituut / Antoni van Leeuwenhoek Ziekenhuis in Amsterdam, Niederlande.
- Akademische Lehrer: H. Braun, F. H. Busse, P. Esquinazi, A. Freimuth, R. Groß, D. Haarer, L. Kramer, H. Kerner, T. Nattermann, F. M. Neubauer, F. Nüsslin, W. Pesch, M. L. Ristig, A. Seilmeier, W. Schnick, W. von Wahl, M. Zirnbauer, J. Zowe.